frontiers in Marine Science

ORIGINAL RESEARCH
published: 18 June 2019
doi: 10.3389/fmars.2019.00306

Correction Factors for $\delta^{18}O$-Derived Global Sea Surface Temperature Reconstructions From Diagenetically Altered Intervals of Coral Skeletal Density Banding

Mayandi Sivaguru[1,2†], Kyle W. Fouke[1,2,3†], Lauren Todorov[1,2,4], Michael J. Kingsford[5], Kaitlyn E. Fouke[6], Jeffrey M. Trop[3] and Bruce W. Fouke[1,5,7,8,9]*

[1] Carl R. Woese Institute for Genomic Biology, University of Illinois at Urbana–Champaign, Urbana, IL, United States, [2] Carl Zeiss Labs@Location Partner, Carl R. Woese Institute for Genomic Biology, University of Illinois at Urbana–Champaign, Urbana, IL, United States, [3] Department of Geology and Environmental Geosciences, Bucknell University, Lewisburg, PA, United States, [4] School of Molecular and Cellular Biology, University of Illinois at Urbana–Champaign, Urbana, IL, United States, [5] Marine Biology and Aquaculture, College of Science and Engineering, ARC Centre of Excellence for Coral Reef Studies, James Cook University, Townsville, QLD, Australia, [6] Department of Biology, Denison University, Granville, OH, United States, [7] Department of Geology, University of Illinois at Urbana–Champaign, Urbana, IL, United States, [8] Department of Microbiology, University of Illinois at Urbana–Champaign, Urbana, IL, United States, [9] Roy J. Carver Biotechnology Center, University of Illinois at Urbana–Champaign, Urbana, IL, United States

OPEN ACCESS

Edited by:
Tamotsu Oomori, University of the Ryukyus, Japan

Reviewed by:
Thomas M. DeCarlo, The University of Western Australia, Australia
Ryuji Asami, Tohoku University, Japan

***Correspondence:**
Bruce W. Fouke
fouke@illinois.edu

† These authors have contributed equally to this work and share first authorship

Specialty section:
This article was submitted to Coral Reef Research, a section of the journal Frontiers in Marine Science

Received: *25 February 2019*
Accepted: *23 May 2019*
Published: *18 June 2019*

Citation:
Sivaguru M, Fouke KW, Todorov L, Kingsford MJ, Fouke KE, Trop JM and Fouke BW (2019) Correction Factors for $\delta^{18}O$-Derived Global Sea Surface Temperature Reconstructions From Diagenetically Altered Intervals of Coral Skeletal Density Banding. Front. Mar. Sci. 6:306. doi: 10.3389/fmars.2019.00306

Reconstruction of sea surface temperature (SST) from the $\delta^{18}O$ and Sr/Ca composition of coral skeletal density banding (CSDB), identified with x-ray diffraction and micro computed tomography, provides invaluable centuries-long records of ocean circulation and climate change. Comparison with age-equivalent instrument measurements of SST over the last 125 years has proven these $\delta^{18}O$-derived SST reconstructions to be generally reliable. However, notable exceptions occur within discrete CSDB stratigraphic intervals that yield $\delta^{18}O$-derived SST underestimates of as much as 9°C with respect to instrument measured SST. Here we combine high-resolution optical and electron microscopy with geochemical modeling to establish correction factors for the impact of marine seafloor physical, chemical, and biological alteration (*diagenesis*) within these altered intervals of CSDB stratigraphy. Four cores were collected from *Porites* coral heads across a 4–24 m water depth bathymetric transect at Myrmidon Reef, Great Barrier Reef, Australia. Precise mapping of diagenetic aragonite cementation was completed within CSDB patterns digitally overlaid on 35 petrographic thin sections fully covering 2.1 m of core. The vast majority of core skeletal material exhibited little to no diagenetic aragonite cementation. However, extensive diagenetic alteration was observed within discrete CSDB intervals near the base of the two deeper water *Porites* heads. This diagenesis serves to modify skeletal density and CSDB stratigraphy in these intervals, as well as structurally reinforce the coral skeleton. Reliable $\delta^{18}O$-based SST correction factors for these diagenetically altered CSDB intervals are established here by applying the percent mixing of diagenetic aragonite cement to a binary mixing model. This approach, with quantitative extents of mixing established with both microscopy and

existing globally distributed coral $\delta^{18}O$ and Sr/Ca data sets, accurately restores modern and fossil coral $\delta^{18}O$-derived SST records. Results indicate that as little as 5% mixing of diagenetic aragonite cement with original coral skeleton will cause $\delta^{18}O$-based SST anomalies of 0.9°C.

Keywords: correction factors, sea surface temperature, coral skeletal density banding, diagenetic alteration, marine carbonate geochemistry, *Porites*, paleoclimate reconstruction, paleothermometry

INTRODUCTION

The record-breaking warm period of 2015 through 2018 continues the dramatic climb of average Earth temperatures over 17 of the last 18 years (Blunden and Arndt, 2016; NASA-GISS, 2018; NOAA-NCDC, 2018). It is therefore increasingly vital to accurately predict future global warming as a means to guide societal planning to survive the environmental impacts of sea level rise, ocean acidification, drought, disease and fire (Hoegh-Guldberg et al., 2007; Barkley et al., 2015). The efficacy of climate change forecasts is determined in large part by comparison of modeling results with past multidecadal and millennial temperature changes recorded in environmental records (*proxies*) such as lake and ocean sediments, tree rings and ice (IPCC, 2018). Especially critical in this regard are the changes in sea surface temperature (SST) reconstructed from the $\delta^{18}O$ and Sr/Ca of $CaCO_3$ (*aragonite*) coral skeletons. Annual high-density band (HDB) and low-density band (LDB) couplets form continuous stratigraphic sequences herein called coral skeletal density banding (CSDB). These CSDB sequences provide a chronostratigraphic age model that is interpolated with the SST reconstructed from the skeletal $\delta^{18}O$ and Sr/Ca. These combined geochemical and age proxies are the only means to reconstruct high-frequency seasonal changes in local and regional ocean circulation and climate, such as the El Niño–Southern Oscillation (ENSO) (Lough and Barnes, 1989; Alibert and McCulloch, 1997; De'ath et al., 2009; Alpert et al., 2016; IPCC, 2018).

Chronostratigraphy provided by CSDB, as identified with x-ray diffraction (XRD) and micro computed tomography (MicroCT), is the primary contextual temporal framework used to reconstruct and globally correlate the timing and magnitude of past changes in SST (Knutson et al., 1972; Alibert and McCulloch, 1997; Gagan et al., 1998; Correge, 2006; Moses et al., 2006; Hendy et al., 2007; DeCarlo et al., 2018). Centuries-long SST paleothermometry is reconstructed from the $\delta^{18}O$ and Sr/Ca skeletal chemistry preserved within these CSDB stratigraphic sequences. The fidelity of CSDB-derived SST is evaluated via direct comparison with age-equivalent instrument measurements of SST collected over the last 125 years. Overall, this has proven CSDB-derived SST to be generally reliable, providing the proof-of-concept required to defend application of $\delta^{18}O$-derived SST paleothermometry to much older CSDB sequences where there is no independent instrument check of SST (Lough and Barnes, 1989; Alibert and McCulloch, 1997; Cohen and Hart, 2004; DeLong et al., 2007; De'ath et al., 2009; Nurhati et al., 2009; Sayani et al., 2011; Alpert et al., 2016). At the same time, these reports have also observed that SST reconstructions from some CSDB intervals underestimate age-equivalent instrument-measured SST by as much as 9°C. These anomalies have primarily been interpreted to reflect a variety of complex processes. For instance, while skeletal HDB and LDB layering is strongly influenced by coupled coral and zooxanthellae physiological responses to seasonal changes in SST, the formation of CSDB sequences is also sensitive to other abiotic ecological parameters such as lunar cycles, solar radiation and fresh-water runoff, as well as instrument error (Barnes and Lough, 1993; DeCarlo and Cohen, 2017). Changes in skeletal growth rate and other biological "vital effects" during biomineralization can also skew $\delta^{18}O$-derived SST (Lough and Barnes, 1989; Alibert and McCulloch, 1997; Gagan et al., 1998; Cohen and McConnaughey, 2003; Cohen and Hart, 2004; Sayani et al., 2011; Alpert et al., 2016). These changes can cause variations in $\delta^{18}O$-derived SST that are large enough (as much as 2–6°C) that they prevent the identification of individual ocean events (Gagan et al., 1998; Crowley et al., 1999; DeLong et al., 2007; Alpert et al., 2016). In addition, changes in Sr/Ca have also been linked to differential growth rates between individual "fans of corallites" and observed to create anomalies of 1 to 3°C (Alibert and McCulloch, 1997).

Another especially critical factor is that coralla undergo early post-depositional physical, chemical and biological alteration in the marine seafloor environment in which they originally grew (*diagenesis*) (Potthast, 1992; Cohen and Hart, 2004; Muller et al., 2004; Quinn and Taylor, 2006; Nothdurft and Webb, 2007; Perrin and Smith, 2007; McGregor and Abram, 2008; Sayani et al., 2011; Sadler et al., 2014). The thickness, lateral continuity, intensity and overall stratigraphic layering patterns are all vulnerable to seafloor diagenetic alteration in specific CSDB intervals. However, the extent to which seafloor diagenetic alteration takes place within any given CSDB stratigraphic interval is dependent upon the relative volume of seawater that fluxes through the porous coral skeleton (Banner and Hanson, 1990). In addition, the extent of diagenetic alteration of coral skeletons also depends strongly on multiple other interacting parameters including aragonite crystalline structure and chemistry, biological activity, biotic and abiotic surface chemistry, surface area and roughness, age of the skeleton, and changing marine environmental conditions (Berner, 1966; Morse and Mackenzie, 1990; Kandianis et al., 2008; Walther et al., 2013). As a result, from the perspective of marine carbonate sedimentology and geochemistry, it is expected that the effects of seafloor diagenesis would be heterogeneously distributed within any given corallum (Berner, 1966; Banner and Hanson, 1990; Morse and Mackenzie, 1990; Tucker et al., 1990; Fouke et al., 1996). Therefore, it is likely that the majority of a corallum is diagenetically unaltered, while specific CSDB intervals exhibit

extensive diagenetic alteration. This stratified distribution of diagenetic impact is consistent with the discrete intervals of δ^{18}O-derived SST anomalies reconstructed from previous studies of coral skeleton cores from around the world (Lough and Barnes, 1989; Alibert and McCulloch, 1997; Cohen and Hart, 2004; DeLong et al., 2007; De'ath et al., 2009; Nurhati et al., 2009; Sayani et al., 2011; Alpert et al., 2016).

Our study, which directly builds upon previous research, is the first to fully contextualize and integrate high-resolution microscopy with mass balance binary mixing models to establish reliable and reproducible correction factors for the impact of seafloor diagenesis on δ^{18}O-derived SST. Four cores are analyzed from *Porites* coralla growing at 4–24 m water depth (WD) at Myrmidon Reef, Great Barrier Reef, Australia (**Figure 1**). This includes detailed study of 35 polished 25 μm-thick thin sections covering a total core length of 2.1 m. While more than 95% of the coral skeletal cores exhibit little to no diagenetic alteration, the bottom several centimeters of the two deeper cores (16 and 24 m WD) contain CSDB intervals of extensive diagenetic aragonite cementation within original skeletal pore spaces. We derive correction factors for δ^{18}O-based SST reconstructions by applying the percent mixing of diagenetic aragonite cement with original skeleton (as determined from high-resolution microscopy) to binary mixing models. These correction factors are directly applicable to CSDB-derived δ^{18}O and Sr/Ca data sets from the skeletons of other types of corals and other marine invertebrates from around the world.

MATERIALS AND METHODS

Sample Location and Collection

Coral skeletal cores were collected under the Australian Government Great Barrier Reef Marine Park Authority Permit G15/37167.1 issued to M.J. Kingsford. Four colonies of *Porites* growing at 4–24 m water depth (WD), measured from the seafloor and acknowledging that mean high water (MHW) can be 1.5 m (data Pith Reef, Australian Hydrographic Service), were cored with a 6 cm-diameter stainless steel pneumatic drill that was operated using standard SCUBA techniques on Myrmidon Reef (18°15′56″ S, 147°23′21″ E), Great Barrier Reef, Australia (**Figure 1**). Myrmidon is the most seaward reef of the Great Barrier Reef, located 124 km from the Townsville harbor. This required a week-long expedition on a live-aboard ship in order to complete the coral core collection. A total of 35 polished 25 μm-thick thin sections were prepared from the four cores (**Figure 2**). The cores were gently bleached in 1% hydrochloric acid to remove coral tissue, air dried, carefully packaged and shipped to Illinois.

XRD and MicroCT Analyses

Intact cores were imaged at ∼60 μm-resolution on a custom-designed MicroCT system (North Scientific Instrument, Feinfocus 225 kV) in the University of Texas Computed Tomography (UTCT) high-resolution x-ray imaging facility. After acquiring the 3D data, each core was cut through the center into vertical 5 mm-thick and 2 mm-thick slices. The 5 mm-thick slices were also imaged using a standard XRD (Siemens Model #10092624, 70 kV) system at the Veterinary School of Medicine at the University of Illinois Urbana-Champaign. Further details are presented in the extended **Supplementary Methods** section. For all of the XRD and MicroCT images presented in this study, the lighter more highly exposed layers are high density bands (HDBs) and the darker less exposed layers are low density bands (LDBs) equivalent to the black background.

Thin Sectioning

From the central 5 mm-thick core slices, a total of 35 billets were cut, distributed over 2.1 m of the entire 2.3 m length of all four cores (representing 90% coverage). From each billet, an ultrathin 25 mm-thick ultra-thin section was prepared at Wagner Petrographic, Linden, Utah. Each thin section was impregnated with blue-dyed epoxy, doubly polished and mounted onto standard biological-sized glass slides. Further details are in the extended **Supplementary Methods** section.

Optical Microscopy

A suite of integrated optical microscopy techniques were applied to determine the crystalline structure of the *Porites* coral skeletal cores in thin section. This included the first integrated application to coral skeletons of the suite of Airyscan super-resolution auto-fluorescence microscopy (SRAF), bright field (BF), dark field (DF), polarization (POL), phase-contrast (PC), and ring aperture contrast (RAC) techniques (Sivaguru et al., 2012, 2018a,b). XRD and MicroCT digital transparencies were directly overlaid on images collected from each of these modalities for each thin section to determine the precise position of HDBs and LDBs, and conduct optical microscopy (140–250 nm-resolution) within the context of the CSDB stratigraphic sequences. These analyses were then complimented by screening with scanning electron microscopy (SEM). The suite of instruments, with the appropriate optical magnifications to render an ultimate spatial resolution of 250 nm, included: (1) Zeiss Axio Zoom.V16 microscope with a 1.0× Plan Apochromat NA 0.25 objective (for BF, BF-EDF, DF); (2) Nanozoomer whole slide scanner system with an Uplansapo 20×, 0.75 NA objective (for BF); (3) Zeiss AxioObserver Z.1; 20× Plan Apochromat 0.8 NA, 63× Plan Apochromat 1.4 NA Ph3 objectives (for BF, PC, POL); and (4) Zeiss Axioscan Z1 whole slide scanning system with 20×, Plan Apochromat 0.8 NA and 50× Plan Neofluar 0.95 NA POL objectives (for BF, POL, and RAC). All optical microscopy was conducted on instruments housed in the Microscopy and Imaging Core Facility of the Carl R. Woese Institute for Genomic Biology on the University of Illinois Urbana-Champaign campus. This facility was the first North American laboratory to be selected as a Zeiss Labs@Location Partner by Carl Zeiss LLC. Further details are in the extended **Supplementary Materials** section. In addition, laser transmitted images and Airyscan SRAF (super-resolution autofluorescence) images were obtained as described previously (Sivaguru et al., 2018a) using a Zeiss LSM 880 Airyscan system.

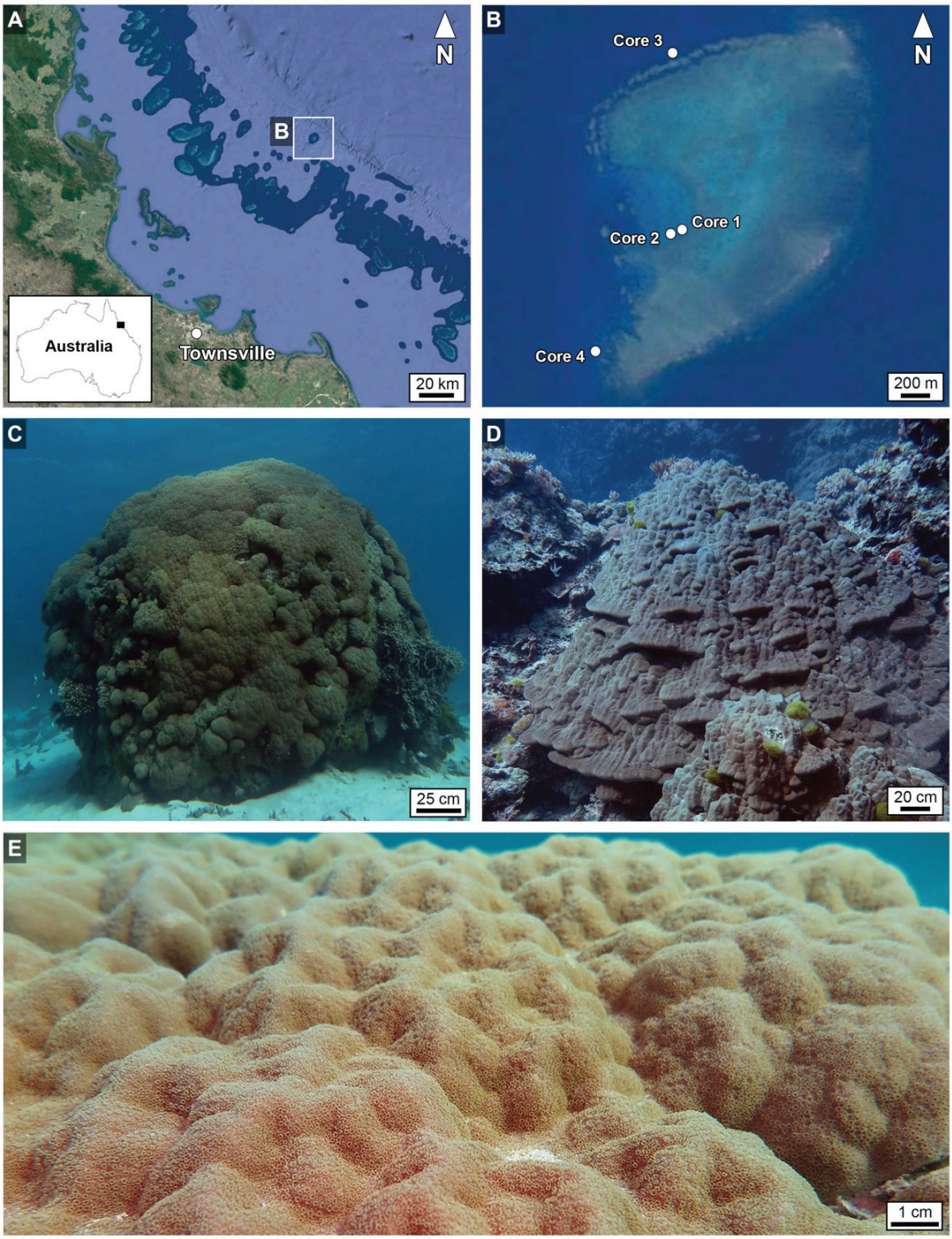

FIGURE 1 | (A,B) Geographic location of Myrmidon Reef in northeast Queensland, Australia (CSIRO), showing specific locations of *Porites* coralla from which Cores 1–4 were collected. **(C,D)** Field photographs of the coralla from which Core 2 **(C)** and Core 3 **(D)** were drilled. **(E)** Field photograph of the bumpy living tissue-covered growing surface of the *Porites* corallum shown in **(C)**. The images **(A,B)** are made in a ArcGIS software (Economic and Social Research Institute, ArcGIS version 10.5) at the Department of Geography and Geographic Information Science, University of Illinois at Urbana-Champaign; https://www.geog.illinois.edu/giscience). The map inset of the Australian coastline in image A was traced from open source Google Maps (https://www.google.com/maps/@-25.2072384,138.5384141,4.74z) using Canvas Draw 4 for Mac.

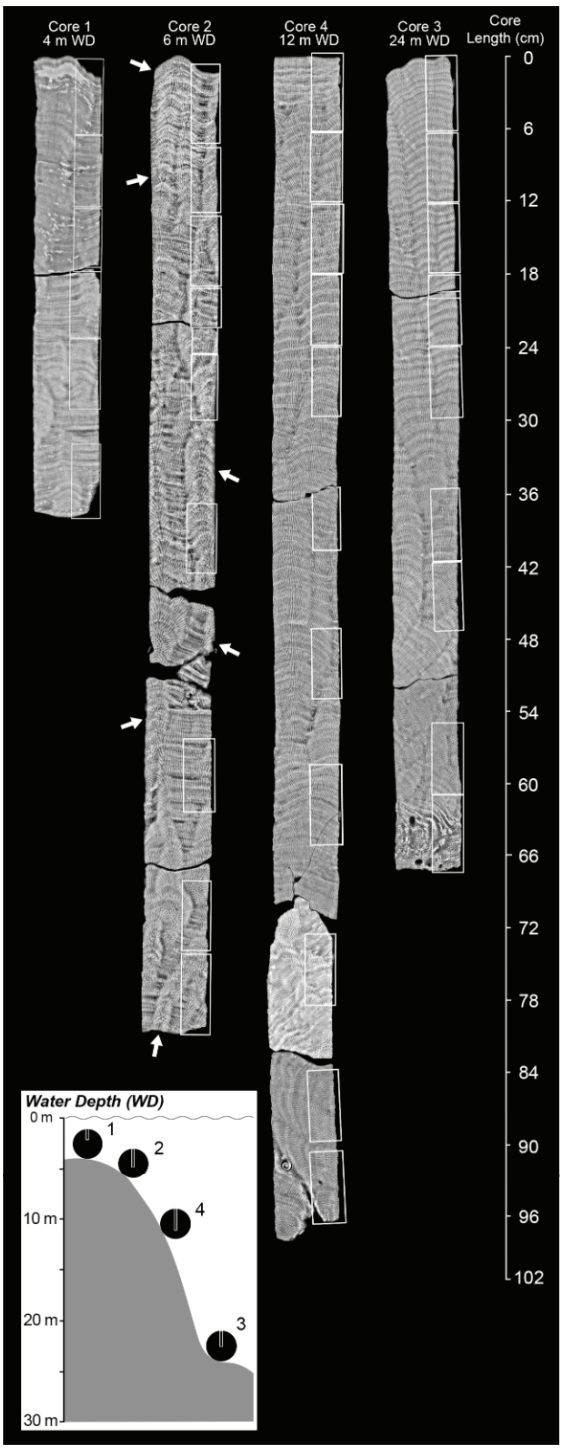

FIGURE 2 | Maximum intensity projection of microcomputed tomography (MicroCT) from 2 mm-thick equivalent slices (a total of 28 slices each having 69 μm isodiametric voxel size per slice) oriented vertically through the center of four *Porites* cores from Myrmidon Reef, Great Barrier Reef, Australia. Cores broke into segments while drilling and are shown in their original vertical alignment. White boxes indicate the position within each core from which 35 petrographic thin sections were prepared and analyzed. The total length of core covered by thin sections is ∼2.1 meters. Coral skeletal density banding (CSDB) layering patterns, while often nearly horizontal and concave-downward (top of Core 4), can also exhibit vertical and concave up orientations (base of Cores 3 and 4). White arrows show spiraling corallites bundles (**Supplementary Data Movies S1a,b**) that are expressed as cm-scale bumps on the uppermost growing corallum surface. Lower left insert is a schematic cross-section of the bathymetric distribution of the four *Porites* coral heads cored in this study. The four coralla are distributed around Myrmidon Reef at the indicated depths and are not along a single transect. White boxes show the position and depth of the cores drilled within coralla. Core numbering reflects the sequence in which they were cored.

Scanning Electron Microscopy

Scanning electron microscopy was used to determine ultra-fine details of *Porites* coral skeleton crystalline architecture as a corollary to thin section imaging. Intact slices of coral core billets, both before and after etching with 0.1% formic acid for 30 or 90 s (Nothdurft and Webb, 2007), were sputter coated for 70 s, terminated in water and dried in an oven (60–65°C) with a gold palladium (Au/Pd) target using a Denton DESK II TSC sputter coater (Denton Vacuum, Turbo Sputter Coater, Moorestown, NJ, United States). The samples were then imaged under a FEI Quanta FEG 450 FESEM (Hillsboro, OR, United States) at specific magnifications to illustrate coral skeleton crystal structure across multiple length scales. Further details are in the extended **Supplementary Methods** section.

Whole Thin Section Slide Scanning and Porosity Analysis in HDBs and LDBs

HDB and LDB porosity was calculated from quantitative analyses of 420 high-resolution BF images collected at 250 nm-resolution from across all 35 thin sections in each of the four *Porites* cores (**Figure 2**). Porosity of HDBs and LDBs was calculated from 40× Nanozoomer images of each of the 35 thin sections from all four cores using the Zeiss AxioVision program (version 4.9.1), with point-by-point data spreadsheets analyzed in Excel data (**Supplementary Material Data S1**). A porosity analysis macro program was created by defining a "rectangle outline" to determine the correct red, green, blue color range (8-bit gray scale) for each image. Due to slight differences in section thickness, the colors of the epoxy tones varied from light blue to dark blue. As a result, a range of blue shades were used to define and select regions of skeletal porosity. This color range was recorded for each thin section to complete the porosity calculation and determine an overall range of blue thresholds. The program calculates the total number of blue pixels (within the thresholds) and normalizes this value to the full frame yielded porosity value for each image. A total of 420 images (12 images were collected from each of 35 thin sections) were analyzed for HDBs (n = 210) and LDBs (n = 210) from top-to-bottom in all cores. The mean and standard deviation of these porosity measurements was determined by averaging all of the images within a HDB or LDB specifically defined by BF petrography. Percent porosity for a given thin section was determined by normalizing the porosity value to the full image dimension (see **Supplementary Material Data S1**). The percent (%) porosity

values and their plus-or-minus standard deviation is shown as scatter plot, with the depth in centimeters within each core (linked to middle of each thin section) is shown along the X axis. Statistics and plotting was completed with Sigma Plot 11.0 (Systat Software, Englewood Cliffs, NJ, United States) and assembled in Adobe Photoshop (Adobe Systems, San Jose, CA, United States).

Image Adjustments, Analysis and Presentation

The techniques used to process the 3D Micro CT images is presented above. All SEM images were presented without any intensity corrections. All optical microscopy images were processed in native Zeiss Zen Black (Airyscan) or Zen Blue (all other modalities) software. The entirety of raw data collected for each image presented in this manuscript is available upon request and has also been uploaded to the Figshare website as described in the manuscript. The images are adjusted after following the ethical procedures as described previously (Cromey, 2010). RGB curves were adjusted and presented as linear or with a gamma adjustment of 0.4–0.5, min/max, best mode or manually adjusted in the display properties window in the Zeiss Zen software for representative brightness, contrast and clarity. Final images are cropped, aligned, resized and in some cases the opacity has been changed to show the details of overlay of images in two different modalities, where necessary. All of these adjustments were performed in Adobe Photoshop (Adobe systems, San Jose, CA, United States). In addition, for 3D visualization of MicroCT was completed to create 3D images and movies using Imaris 3D Visualization software (Bitplane, Zurich, Switzerland) or Avizo.

Binary Mixing Model

High-resolution microscopy was combined with binary mixing modeling to quantitatively estimate the impact of seafloor diagenesis on sea surface temperature (SST) paleothermometry reconstructions. A binary mixing line was calculated from Langmuir et al. (1978) shows changing Sr/Ca mmol/mol vs. δ^{18}O VPDB with increased mixing of original coral skeleton aragonite with diagenetic aragonite cements. The extent of mixing is independently and quantitatively determined from microscopy of the coral skeleton. Endmember geochemical compositions for the original Porites aragonite skeleton (δ^{18}O = −5.5 VPDB; Sr/Ca = 8.7 mmol/mol) and diagenetic aragonite cement (δ^{18}O = −2.0 VPDB; Sr/Ca = 10.5 mmol/mol) are from analyses of *Porites* in Papua New Guinea (Quinn and Taylor, 2006). The gray data field (n = 80) are all data from Quinn and Taylor (Quinn and Taylor, 2006). Importantly, Quinn and Taylor made the invaluable presumption of mixing during sampling between the original coral skeleton (which they call "pristine coral") and the endmember diagenetic aragonite cements (which they call "abiotic aragonite"). However, they did not quantitatively model the data to prove mixing, nor did they correlate these analyses with quantitative petrography of the coral skeleton. As a result, they could not establish a quantitative correction factor for δ^{18}O-derived SST required for physical mixing effects during sampling. In the present study, the X-axis and Y-axis intercepts indicate the amount of change caused by mixing in Sr/Ca mmol/mol and δ^{18}O VPDB, respectively. These shifts in isotopic and elemental composition can then be used to correct SST reconstructions. A δ^{18}O VPDB SST corrections follow previously established paleothermometry calculations (Epstein et al., 1953; Kim and ONeil, 1997; Nurhati et al., 2009; Sayani et al., 2011; Kim et al., 2015). These indicate SST corrections of +3.6°C for 21% mixing, +7.1°C for 43% mixing, and +9.3°C for 53% mixing, respectively.

Primary Skeleton and Cement Mixing Thresholds

The BF images from bottom 6 cm of HDBs at multiple locations in the base of Cores 3 and 4 were used for extracting a range of cement and primary skeleton mixing ratios. Using Core 3 as an example, a red circle with an area of 1 mm was drawn to represent the typical 1 mm-diameter drill tip. Then the images were thresholded based on the RGB values of the blue color epoxy used for the thin sectioning using the 2D image analysis program Axiovision 4.93 (Carl Zeiss, Oberkochen, Germany). The thresholded areas are restricted to inside the 1 mm drill trip by tracing the red line and areas of blue pixels were measured in pixel^2. Then using the same program, areas of the occlusion (cement) together with remaining porosity (blue areas) were traced based on the sclerodermite transition region as a marker. Inside the traces the area in pixel^2 is determined, leaving the primary skeleton. This area is subtracted from the 1 mm drill tip area to assess the primary skeleton area. To calculate the cement area, the blue epoxy area is subtracted from the tracings of sclerodermite traced area, then the percent cement is calculated by using the 1 mm drill trip area over the cement area. Based on these, the absolute skeleton area, cement area and remaining porosity area have been calculated and adding their percent lead up to 100%. The cement area is set at "0" and primary skeleton area set at 100% for the ∼0% location of the HDB. All locations are retrieved from HDB areas at the bottom of Core 3. This data is presented in **Supplementary Material Data S2**.

RESULTS

CSDB Stratigraphy Reflects Growth Morphology

Coral skeletal density banding stratigraphic sequences are cross-sections of corallum morphology that reflect meter-scale whole head hemispherical curvature, centimeter-scale surface topography and millimeter-scale shapes of individual polyp skeletal cups (*corallites*). *Porites* coralla have irregular surfaces that serve to increase surface area and enhance the photosynthetic activity of zooxanthellae living in coral tissues (**Figures 1C–E**, **2**; Piggot et al., 2009; Allemand et al., 2011). Shallow water coralla (<10 m water depth; WD) exhibit a dome shape while deeper water heads (>10 m WD) obtain a more flattened helmet shape to increase light capture (**Figures 1C–E**, **2**) (Smith et al., 2017). Individual 1 mm-diameter corallites are secreted to structurally support individual coral polyp tissues (**Figure 3**). Corallites are grouped into 2 cm-diameter

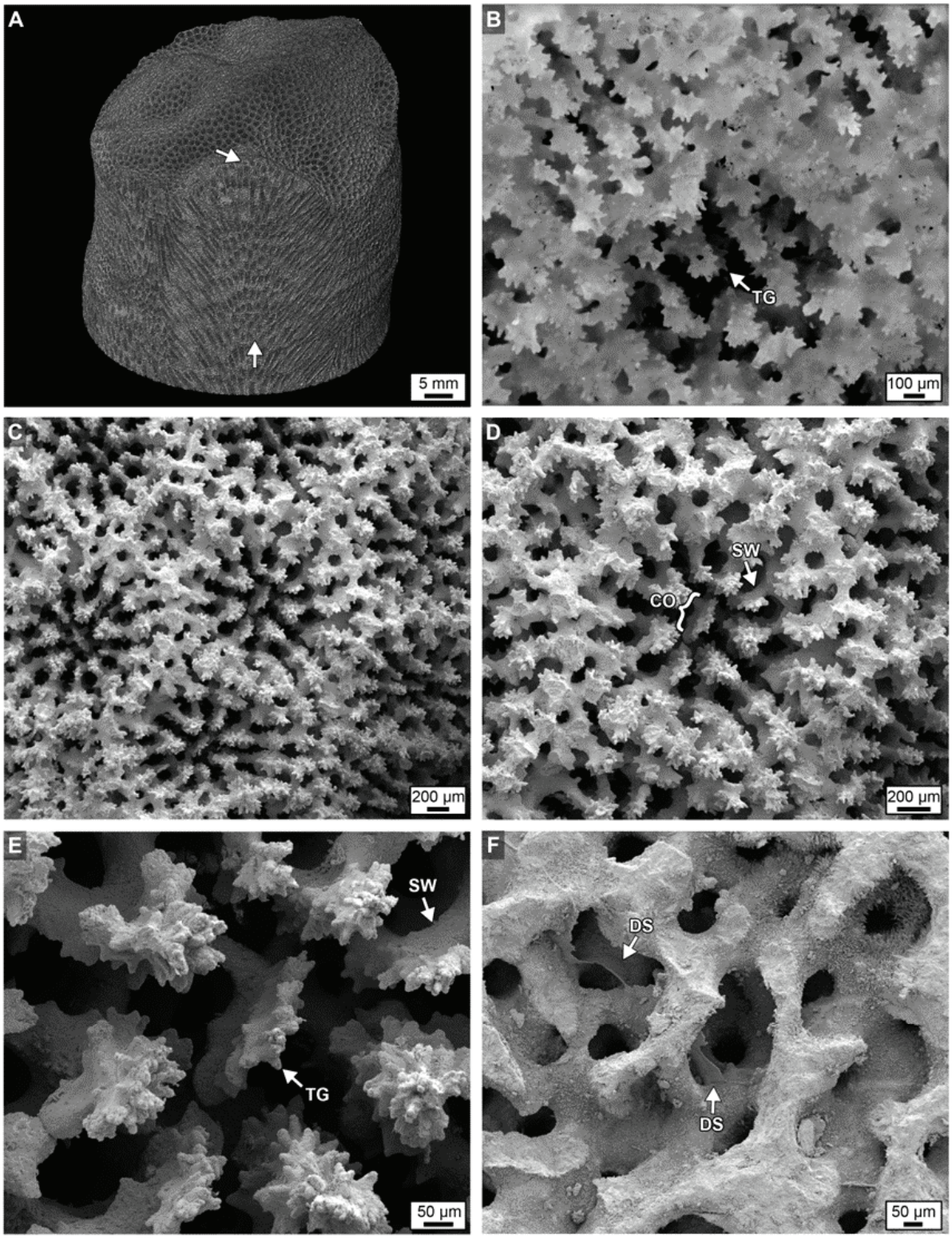

FIGURE 3 | (A) A volume rendered maximum intensity projection of 3D MicroCT image from the top of Core 3 showing spiraling corallite bundles (white arrows) and their bumpy cm-scale surface expression (see also **Supplementary Data Movies S1a,b**). **(B)** An extended depth of focus image under brightfield (BF) of an original *Porites* corallite. **(C–E)** Scanning electron microscope (SEM) images of original *Porites* corallites. **(F)** Scanning electron microscopy (SEM) image of DS within coral skeleton. Labeled components in all images include: CO, columella; SW, skeletal wall; and TG, teeth and granule growing from SW; DS, dissepiments.

spiraling bundles, the tops of which create the bumpy uppermost growing surface of each *Porites* corallum (**Figures 1E**, **3A** and **Supplementary Data Movie S1a**). Cores drilled vertically through the center of large coralla are often expected to have nearly horizontal to concave-down CSDB. However, in practice, vertical to concave up CSDB are common toward the bottom of cores collected from undisturbed *in situ* coralla (**Figure 2**). In addition, spiraling corallite bundles are observed from top-to-bottom in CSDB sequences throughout cores (**Figure 2**). These types of non-horizontal CSDB stratigraphic sequences are created by changing biotic and abiotic environmental factors on the seafloor that cause lateral and vertical shifts in the trajectory of skeletal accumulation through time (Darke and Barnes, 1993).

Original HDB and LDB Skeletal Structure

The top few millimeters of each core is the zero-age accreting surface where living coral tissue is actively secreting pristine skeleton. Corallite skeletal walls in these uppermost surface layers can therefore be considered original crystallization products that result from combined coral tissue cellular controls and environmental influences (Cohen and McConnaughey, 2003; Gower, 2008; Weiner and Addadi, 2011; Von Euw et al., 2017). Our microscopy indicates that HDBs in the uppermost few centimeters of each core have an average porosity of 32% ($\pm$ 7%; n = 210), while LDBs exhibit an average porosity of 60% ($\pm$ 12%; n = 210; **Figure 4**). This is the first study to document that the average porosity difference between HDBs and LDBs is 21–40% lower than adjacent original LDBs (mean of all cores; **Figures 4**, **5–7**). The complex crystalline microstructure of *Porites* skeletons has been studied in detail and combined with molecular analyses to determine the phylogenetic history of the Family Poritidae (Stolarski and Roniewicz, 2001; Nothdurft and Webb, 2007; Budd et al., 2012; Kitano et al., 2014). Corallite morphological features identified in these studies as having the most phylogenetic significance for *Porites* include projections on the top (*teeth*) and side (*granules*) of vertical skeletal walls (Budd et al., 2012); **Figure 8** and **Supplementary Figures S5B–F**). These include vertical walls around the circumference of each corallite (*theca*) and vertical walls inside individual corallites (*septa*; **Figures 3B–F**, **8**). However, it is difficult to consistently discriminate between thecal and septal walls in *Porites* in longitudinal thin section. Therefore, the term "skeletal wall" is used to refer to both thecal and septal walls. Skeletal walls are consistently observed to be thicker within HDBs than in LDBs (**Figures 4**, **9A** and **Supplementary Figures S1–S5**), which is consistent with the lower measured original porosity of HDBs derived from high-resolution image analyses completed in the present study (**Figure 4**). In addition, thin horizontal skeletal elements (*dissepiments*) form at the base of the living coral tissue that are significant in both ecological and life history reconstructions (**Figure 4** and **Supplementary Figure S5**; Lough and Barnes, 1989; DeCarlo and Cohen, 2017).

Within the original coral skeletal walls, multiple 5–20 μm-diameter clusters are observed composed of microcrystalline aragonite (**Figures 5G**, **10A–F**). These regions were originally termed a *center of calcification* (COC) (Ogilvie, 1896) and later an *early mineralization zone* (EMZ) (Cuif and Dauphin, 2005). The more descriptive term COC is adopted here to describe these crystallization fabrics. Fan-shaped arrays (*sclerodermites*) are composed of individual needle-shaped (*acicular*) aragonite crystals that radiate from the COCs and exhibit concentric high-frequency layering (**Figures 10**, **11**; Cohen and McConnaughey, 2003; Cuif and Dauphin, 2005; Holcomb et al., 2009). Super-resolution microscopy of etched skeletal wall thin sections less than 10 μm-thick reveals for the first time in modern corals that *Porites* sclerodermites are composed of 140 nm-thick couplets of dark and light layering (**Figure 12**). These are similar to those observed in human calcium oxalate kidney stones (Sivaguru et al., 2018a) and are consistent with 10–40 nm-thick dark-light layering observed in fossil Triassic-age coral sclerodermites under focused ion beam microscopy (Frankowiak et al., 2013). Sclerodermite layers 2–3 μm in thickness have previously been interpreted to be the result of daily deposition (Cohen and McConnaughey, 2003). If correct, this implies that the *Porites* sclerodermite superhigh-frequency layering might represent hourly or even shorter times of skeletal deposition.

Previous studies have described sclerodermites as arrays of single large orthorhombic crystals of aragonite with unit extinction under polarization (called "fibers") (Pratz, 1882). However, high-resolution optical and electron microscopy in the present study indicates that these fibers are composed of individual bundled acicular aragonite crystals (**Figure 11**; Allemand et al., 2011). Therefore, the term "fiber" will not be used and sclerodermites are utilized instead to describe fan-shaped arrays of acicular aragonite radiating away from their initial COC nucleation sites (**Figures 11A,B**). It is common for groupings of these acicular aragonites to have a shared unit extinction in POL (**Figure 10C**).

Skeletal walls are composed of multiple sclerodermites that grow toward and eventually abut against one another (**Figure 10**). Individual 2–3 μm-thick sclerodermite concentric layers have been described as alternating granular (*microcrystalline*) and acicular aragonite crystals (Holcomb et al., 2009). However, extensive optical and SEM microscopy in the present study indicates that these concentric layers are composed of acicular aragonite crystals, with each horizon having an alternating crystal width (**Figure 11**). No granular aragonite was observed in these alternating layers as described in previous studies (Holcomb et al., 2009). Where multiple sclerodermites grow toward each other, their concentric layers are truncated at the contact margin (**Figures 9B,C**, **11B,C**). The outermost concentric layers within some groupings of these sclerodermites appear to be laterally contiguous between individual sclerodermites that comprise the skeletal walls (**Figures 9B,C**, **11B,C**).

Seafloor Diagenetic Aragonite Cementation

Evidence from super-resolution, optical and electron microscopy proves that more than 95% of the total skeletal volume comprising the four cores exhibit little to no diagenetic alteration. In stark contrast, extensive diagenetic aragonite cementation is concentrated within specific CSDB intervals near the base of

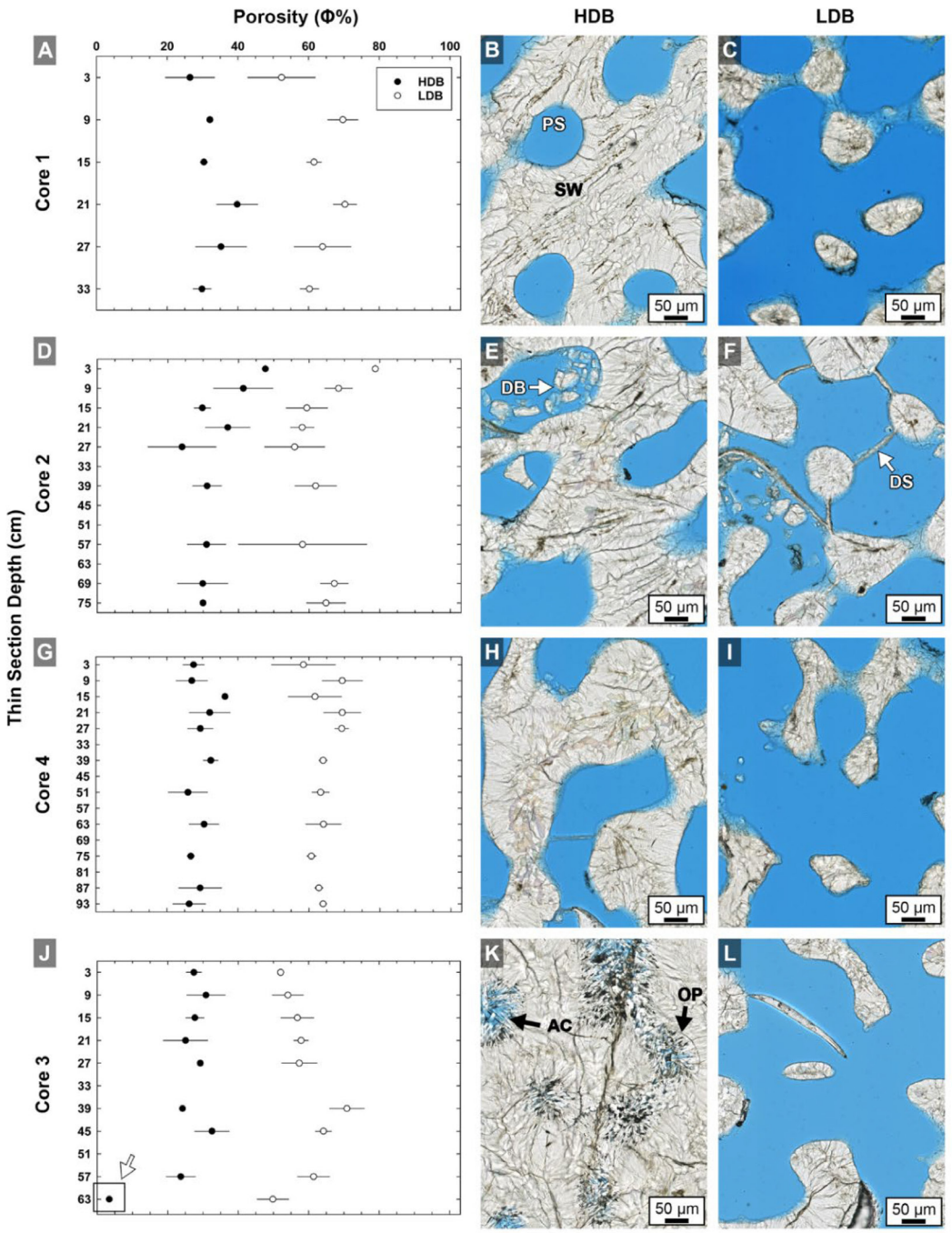

FIGURE 4 | Quantitative analyses of brightfield (BF) high-resolution images (n = 420) of high-density band (HDB) and low-density band (LDB) percent porosity in Core 1 **(A,B,C)**, Core 2 **(D,E,F)**, Core 4 **(G,H,I)**, and Core 3 **(J,K,L)** as analyzed in thin sections from the present study (**Figure 1**). Error bars represent standard deviations of measurements from multiple HDBs and LDBs from several images collected throughout each of the four cores. Analyses include cross-plots of average HDB and LDB porosity versus core depth, as well as example brightfield (BF) images from adjacent HDB and LDB couplet layers. The consistent 28–32% decrease in average HDB porosity is accentuated at the bottom of Core 3 **(K,L)** due to occlusion of porosity by diagenetic aragonite cements (white arrow in graph **J**). Labeled coral skeleton and diagenetic components include: PS, pore space (blue epoxy); SW, skeletal wall; DB, debris; DS, dissepiments; AC, aragonite cement; and OP, original pore margins.

core 3 at 24 m WD and core 4 at 14 m WD (**Figure 4** and **Supplementary Figure S4**). Within these 10 to 15 cm-thick CSDB stratigraphic intervals, the acicular aragonite crystals can reach 100 to 150 µm in length and cause up to 100% skeletal porosity reduction (*occlusion*; **Figures 4–7**, **12B** and **Supplementary Figures S5D–G**). These specific intervals of extensive diagenetic

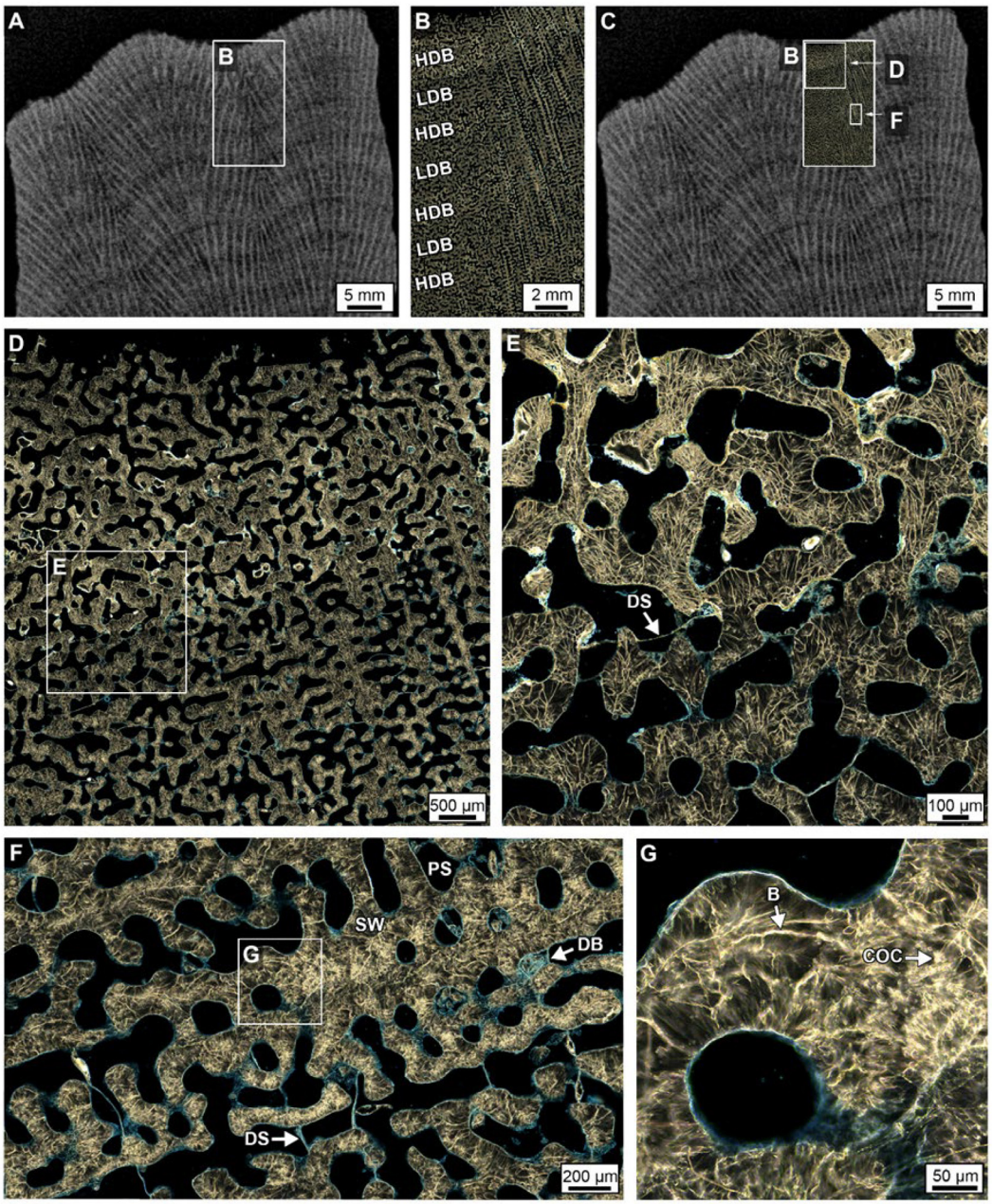

FIGURE 5 | Crystalline structure of high- and low-density bands (HDBs and LDBs) within the uppermost 2 cm of Core 3. **(A–C)** Overlay of a ring aperture contrast (RAC) image on an XRD showing the precise location of coral skeleton density banding (CSDB) on the thin section. **(D,E)** RAC images of an HDB-LDB contact associated with the first dissepiments (DS) below the uppermost growing surface of the corallum. **(F,G)** RAC images (location of **F** shown in **C** and rotated 90°) of an HDB-LDB contact showing bright centers of calcification (COCs) and borings (B).

alteration fundamentally alter HDB and LDB crystalline structure and overall CSDB stratigraphy. The observed increase in the extent of diagenetic aragonite cementation at the base of cores 3 and 4 in deeper seawater at Myrmidon Reef is consistent with previous studies (Schroeder and Purser, 1986; Enmar et al., 2000; Hendy et al., 2007). In addition to analyses of the original structure of coral skeleton precipitated by the living coral tissue, previous studies have documented that several other types of diagenetic alteration fabrics occur such as aragonite needles, rods, encrusted filaments, and botryoids (Nothdurft and Webb, 2007; McGregor and Abram, 2008; Sadler et al., 2014).

High density bands below the uppermost 6 cm in each core have an average porosity of 30% (±7%; **Figure 4**), while LDBs have an average porosity of 62% (±12%; **Figure 4**). As a result, averaged over the entire cores, HDBs have 32% less porosity than LDBs, which is a 4% greater HDB-LDB

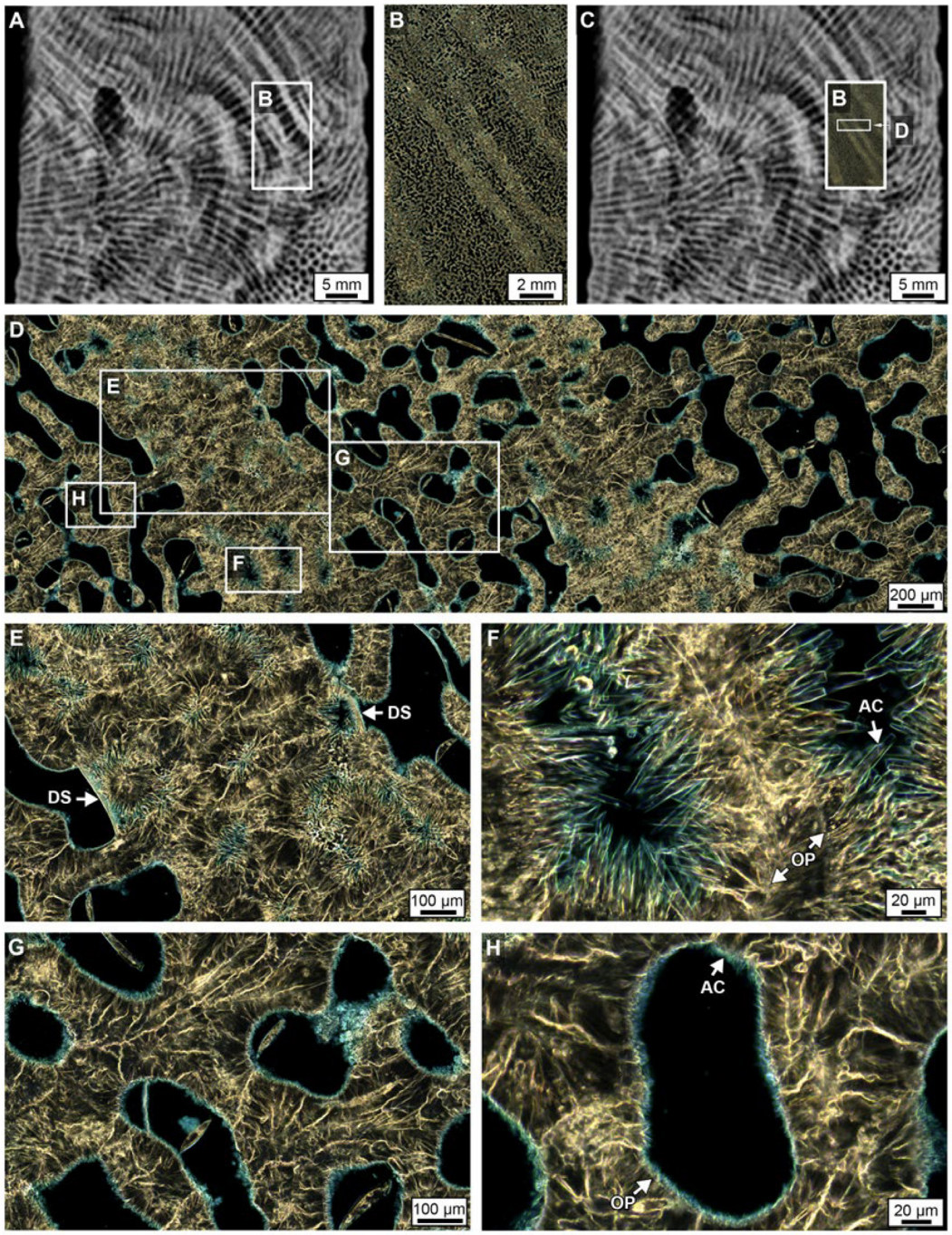

FIGURE 6 | Crystalline structure of high- and low-density bands (HDBs and LDBs) within the lowermost 6 cm of Core 3. **(A–C)** Overlay of a ring aperture contrast (RAC) image on an XRD showing the precise location of coral skeletal density banding (CSDB) on the thin section. **(D)** RAC image of HDBs and LDBs in which HDBs exhibit abundant pore space with diagenetic aragonite cements (AC). **(E)** HDB with dissepiments (DS) bounding AC. **(F)** AC crystals grow from OP into pore space. **(G,H)** High porosity LDB with minimal AC growing inward from the outer pore surface (OP).

reduction than that observed in the uppermost layers of each core (**Figure 4**). The original surfaces of the HDB and LDB skeletal pores exhibit a sharp demarcation of the pore surface in all microscopy modalities (**Figures 4–7**, **9**, **12B** and **Supplementary Figures S5F–G**). This fine line is formed by the termination of radiating acicular aragonite crystals that comprise the skeletal wall sclerodermites. In HDBs, these surfaces are completely encrusted by significantly larger acicular aragonite cements, where the initial abrupt crystal growth contact surface (the original pore space wall) is well-preserved (**Figures 4–7**, **9**, **12B**

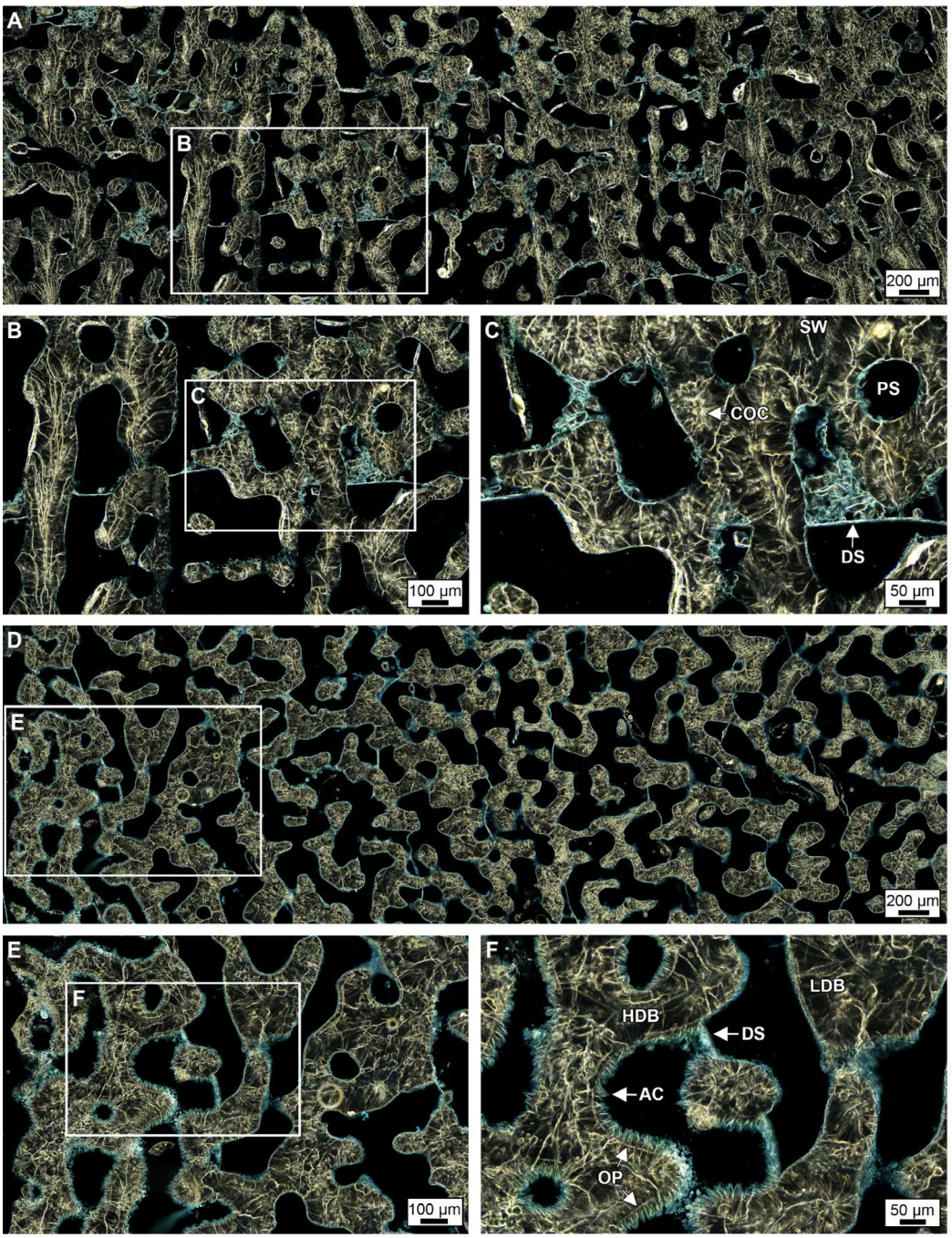

FIGURE 7 | Ring aperture contrast images of crystalline structure and diagenesis in high- and low-density bands (HDBs and LDBs) within the uppermost (top 6 cm, **A–C**) and lowermost 6 cm of Core 4 **(D–F)**. **(A–C)** Overview of a HDB and LDB transition region in the uppermost region of Core 4 with enlargements showing original skeletal pore spaces (PS) with little to no occlusion by acicular aragonite (AC, see enlargement in **C**) and chunks of skeletal debris bound by dissepiments (DS). At the bottom of Core 4 **(D–F)**, extensive diagenetic alteration occurs within discrete HDB stratigraphic intervals with AC partially occluding pore spaces. In addition, diagenetic AC are bound by dissepiments at the transition from HDB to LDB, which is consistent made at the bottom of Core 3 (**Figure 5**).

and **Supplementary Figures S5F,G**). Unit extinction under POL indicates that most of these acicular aragonite cements are syntaxial overgrowths on radiating crystals comprising the original skeletal sclerodermites (**Figures 6**, **10L**, **13**). In addition, these large acicular aragonite cements along the top and bottom of HDBs are sharply bounded by dissepiments (**Figures 4**–**7** and **Supplementary Figure S5E**). LDBs directly above and below these cemented HDBs have significantly fewer and much smaller aragonite cements that only minimally occlude porosity (**Figure 6** and **Supplementary Figure S5**). The high distribution coefficient

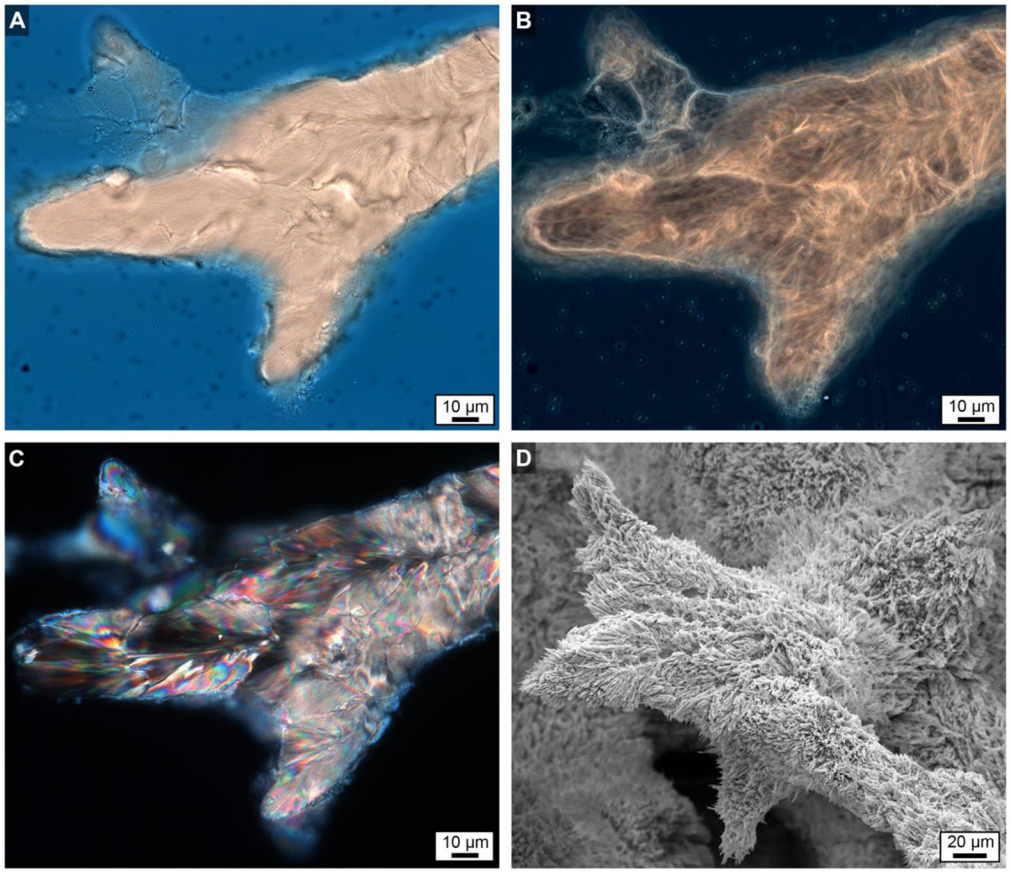

FIGURE 8 | Uppermost growing surface at the top of Core 3 showing finger-like skeletal growth projections. **(A)** Brightfield (BF) image. **(B)** Phase contrast (PC) image. **(C)** Polarization (POL) image. **(D)** Scanning electron microscope (SEM) image taken from a location only mm's away with a strikingly similar morphology to the images shown in **(A–C)**.

of strontium (Sr) for aragonite [DSr > 1; Brand and Veizer, 1980] indicates that increased seawater flux through the skeletal pore spaces is capable of enriching Sr concentrations independently from SST changes. This is consistent with the enrichment of Sr previously observed at the termination of diagenetic aragonite cements in coral skeleton pore spaces (Hendy et al., 2007; McGregor and Abram, 2008; Sadler et al., 2014).

In addition, diagenetic fronts are common that migrate through and solubilize (*dissolve*) original skeletal walls, precipitating a replacement aragonite in its place (*replacement crystallization*) (Bathurst, 1974; McIlreath and Morrow, 1990; Tucker et al., 1990). This process is best illustrated when the original skeleton is only partially diagenetically replaced at its margin (Fouke et al., 1996). Under these circumstances, skeletal replacement begins at the outer margins of the original skeletal wall and progresses inward (*centripetally*) via migrating angstrom- to nanometer-scale zones of dissolution and re-precipitation (**Figures 9D–F**). The leading front of diagenetic replacement is an irregular crystalline margin, behind which fabric-preserving (*mimetic*) replacement crystals are precipitated with distinct characteristics in BF, PC, and POL (**Figures 9D–F**). However, identifying skeletal wall replacement crystallization solely using petrographic data is challenging, unlike the clearly discernable diagenetic aragonite cements precipitated within pore spaces (**Figures 4–7** and **Supplementary Figure S5**).

DISCUSSION

Implications for Future SST Reconstructions From Coral Skeletons

Detailed comparative analyses of all four *Porites* cores from Myrmidon Reef indicate that marine diagenesis is more extensive in deeper water environments and in older down-core portions of each corallum. This distribution is consistent with previous studies (Cohen and Hart, 2004; Quinn and Taylor, 2006). Resulting aragonite cementation and skeletal replacement combine to increase the strength, rigidity, density and overall durability (*rheology*) of each corallum (Hughes, 1987; Fantazzini et al., 2015). These diagenetic processes combine to increase the likelihood of eventual fossil preservation (Hendy et al., 2007), while offsetting the formation of thinner coral skeletal walls and dissolution caused by ocean acidification (Venn et al., 2013; Mass et al., 2017; Eyre et al., 2018).

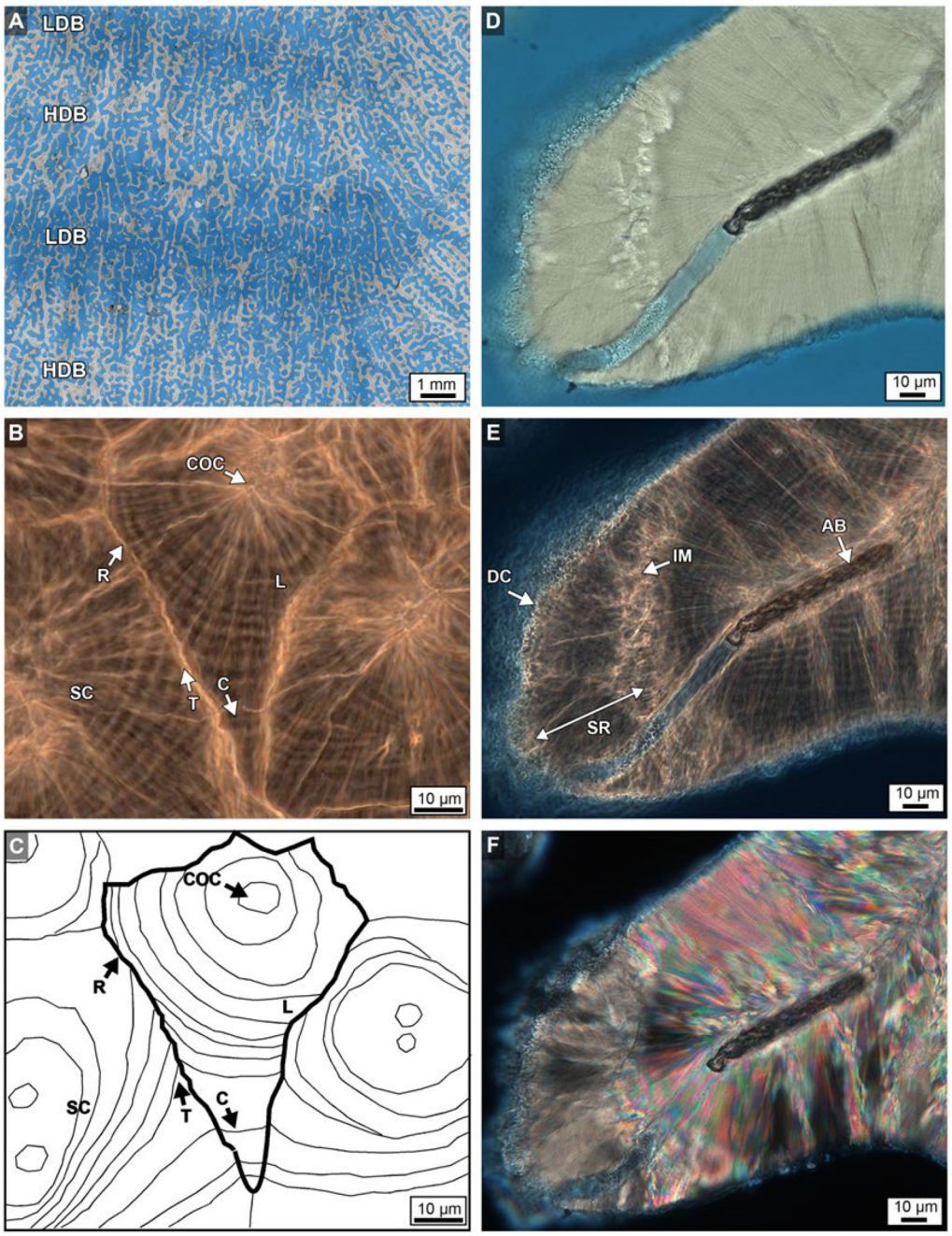

FIGURE 9 | (A) Brightfield (BF) image from near the top of Core 2 overlaid with a transparent XRD image that shows the precise location of high- and low-density bands (HDBs and LDBs). This illustrates the lateral thickening of original skeletal walls within HDBs with respect to LDBs (see also **Figure 4**). **(B,C)** Paired phase contrast (PC) image and its line tracing show the crystalline growth history of multiple sclerodermites (SC) that comprise skeletal walls within the bottom 3 cm of Core 3. Fine concentric layering (L) surrounding individual centers of calcification (COCs) within sclerodermites such as these occur throughout all four *Porites* cores. Layers are truncated (T) at their margins during early growth phases, yet become continuous (C) between sclerodermites during later growth phases. Sclerodermite margins are capped with a fine layer of replacement aragonite (R). BF **(D)**, phase contrast (PC; **E** and **Supplementary Data Movie S2**) and polarization (POL; **F**) images of algal boring (AB), diagenetic cement (DC) and skeletal replacement (SR). The leading edge of the diagenetic replacement front forms an irregular margin (IM).

High-resolution microscopy indicates that coral SST paleothermometry is predominantly impacted by diagenetic aragonite cementation in skeletal pores (**Figures 4–7** and **Supplementary Figure S5**). Similar cementation has been observed in previous petrographic and SEM studies of *Porites* coralla (Quinn and Taylor, 2006; Hendy et al., 2007;

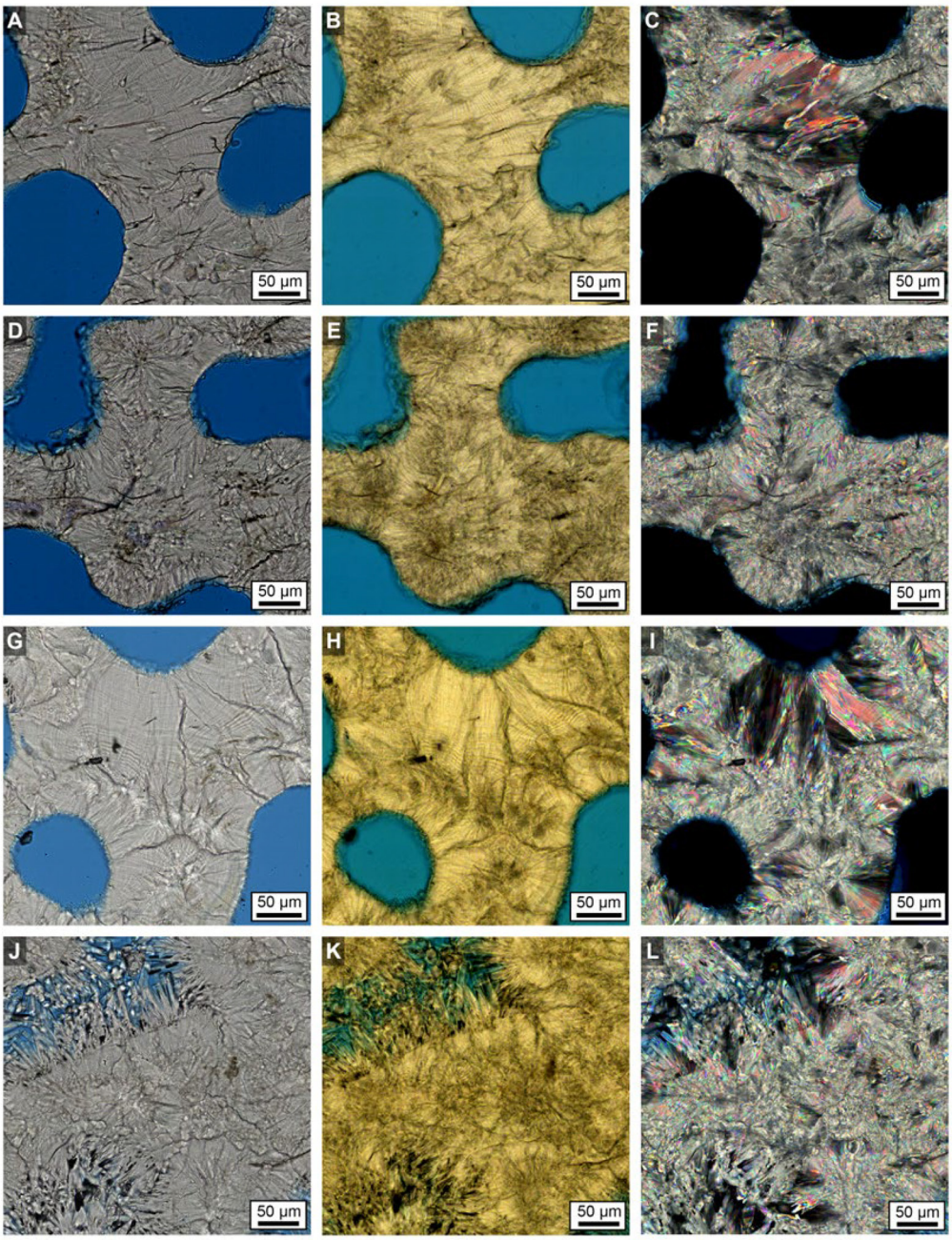

FIGURE 10 | Examples of brightfield (BF; **A, D, G, J**), ring aperture contrast (RAC; **B, E, H, K**) and polarization (POL; **C, F, I, L**) imaging of the crystalline structure of *Porites* original and diagenetically altered skeletons in Core 3. **(A–C)** LDBs in the top 2 cm. **(D–F)** HDBs in the top 2 cm. **(G–I)** LDBs in the bottom 6 cm. **(J–L)** HDBs in the bottom 6 cm.

Nothdurft and Webb, 2007; McGregor and Abram, 2008; Sayani et al., 2011; Sadler et al., 2014). However, the present study is the first to quantify seafloor diagenetic aragonite cementation within specific individual HDBs and LDBs, infer the associated role of diagenesis in driving the redistribution of $CaCO_3$, and fundamentally link these diagenetic effects to the alteration of CSDB sequences across multiple length scales (mm's to m's). There is absolutely no doubt that corals originally deposit skeletal HDBs and LDBs to form continuous CSDB sequences via fundamentally important yet complex relationships with seasonal temperature changes (Wells, 1963; Knutson et al., 1972; Lough and Barnes, 1989, 2000; Brachert et al., 2013; Barkley et al., 2015). As a result, application of Nicholas Steno's 1667 Law of Superposition (i.e., undisturbed stratigraphic sequences have older layers at the bottom and younger layers at the top (Laudan, 1987) creates an invaluable

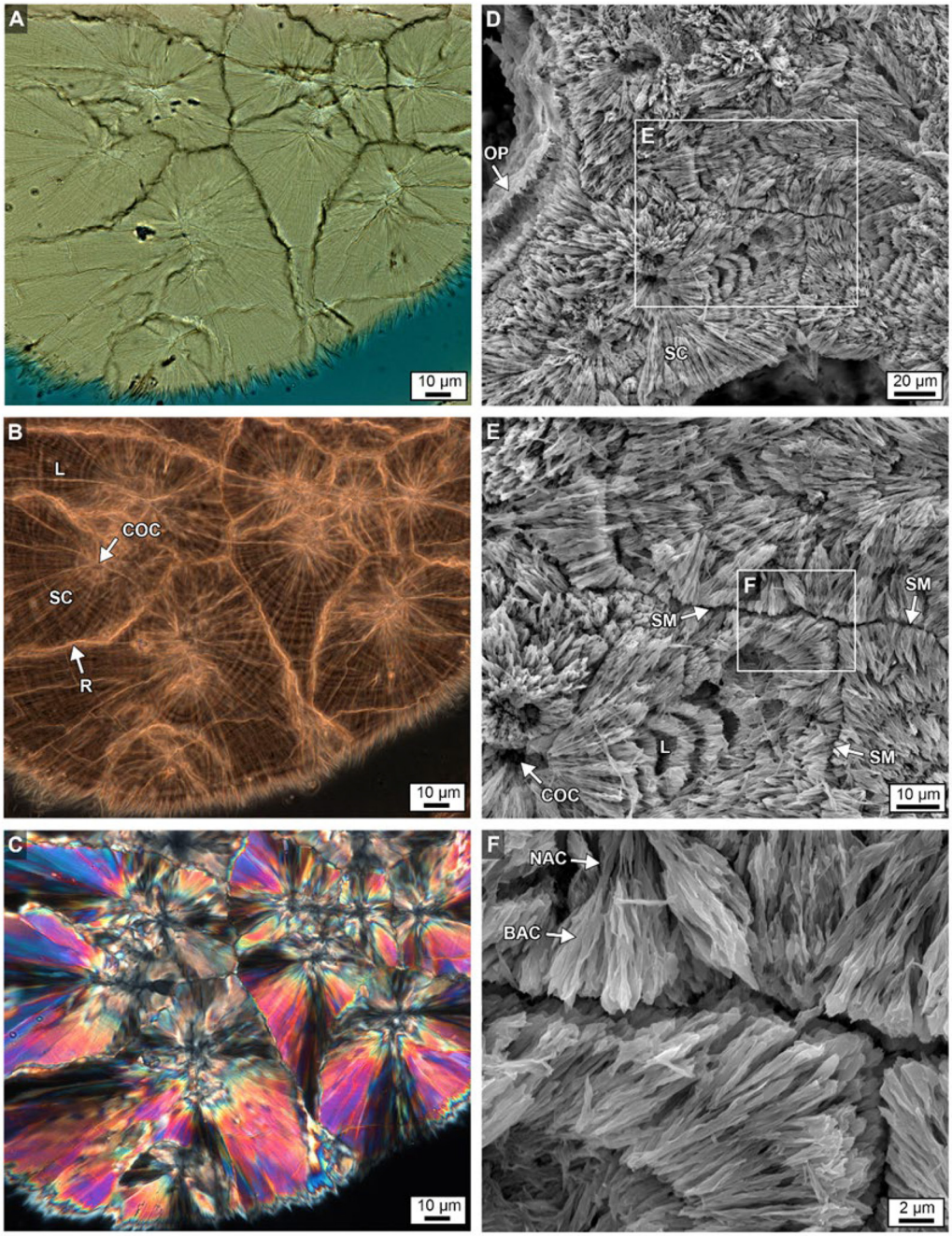

FIGURE 11 | Brightfield (BF; **A**), RAC **(B)**, and polarization (POL; **C**) images of a skeletal wall showing the crystalline growth history of multiple types of sclerodermite (SC) layering from several centers of calcification (COCs) from the bottom 6 cm of Core 3. Details are presented in **Figures 9B,C**. **(D–F)** Complementary images of etched intact skeleton showing similar SC margins, narrow aragonite crystals (NAC) and broad aragonite crystals (BAC) and COCs at increasing levels magnification, with ensuing enlargements from each white box.

relative chronostratigraphic history and correlation tool for coral growth (Lough and Barnes, 1989).

However, microscopy in the present study indicates that seafloor diagenetic alteration of CSDB has the capacity to markedly alter the thickness, intensity, lateral continuity and mineralogical and geochemical character of these CSDB sequences (**Figure 2**). Seafloor diagenetic alteration causes CSDB sequences seen in X-Ray and MicroCT to appear darker and thicker with fewer fine layers of intermediate density (**Figure 2**). This demonstrates that down-core measurement of coral skeletal growth rate through time from CSDB sequences [e.g., De'ath et al. (2009)]. The character and

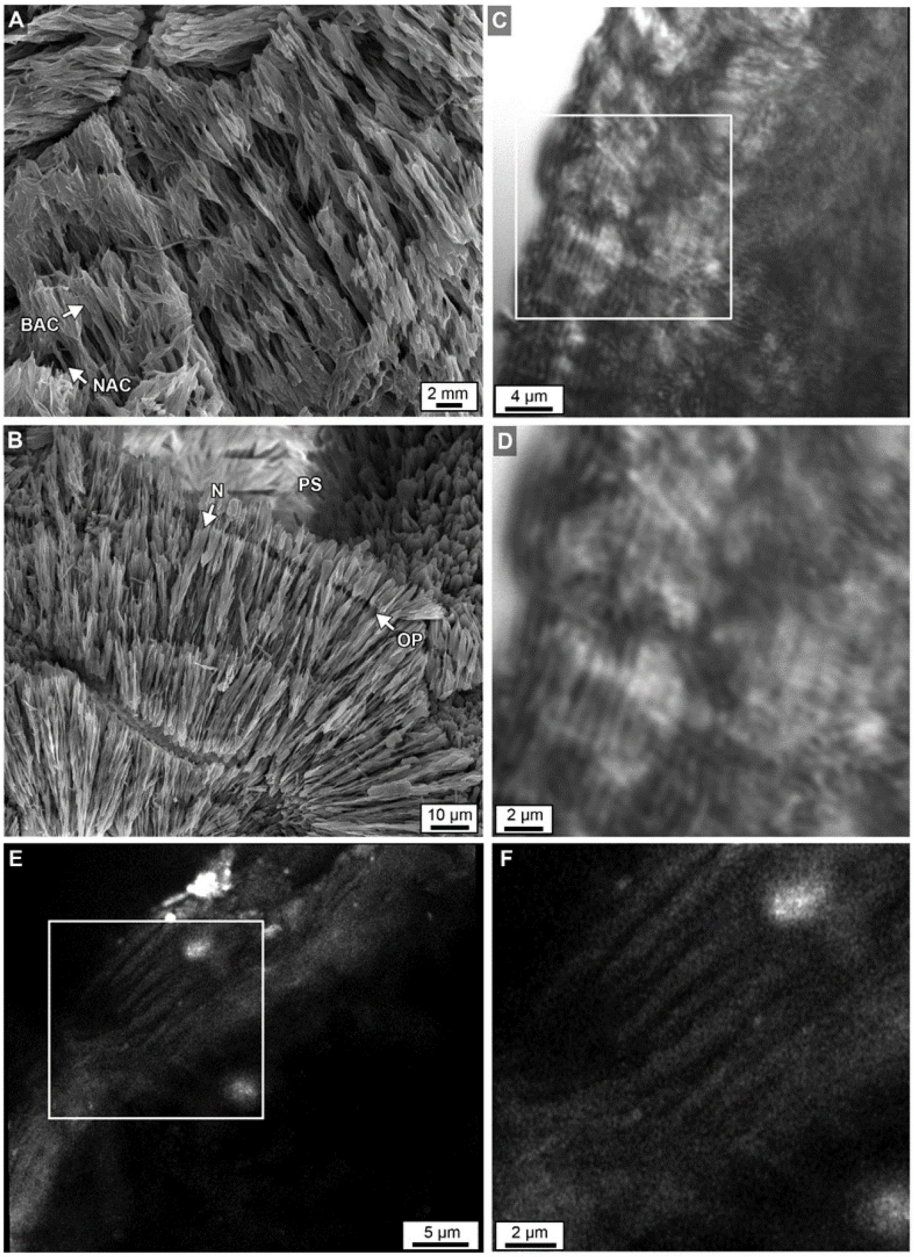

FIGURE 12 | (A) Acicular aragonite morphology making up dark white bands constituting narrow aragonite crystals (NAC) and broad aragonite crystals (BAC) as described in **Figure 11**. **(B)** Margins of original porosity (OP), pore space (PS) and aragonite needles (N) are depicted. **(C)** Laser transmitted light images of etched skeleton at the growing uppermost top surface of Core 3 showing concentric higher frequency (200–250 nm-thick) layering within sclerodermites (dark = organic matter; light = crystalline). **(D)** Magnified image in box **C**. **(E)** Airyscan SRAF image showing organic matter in the same etched skeleton at a different location showing high frequency layering (**Supplementary Data Movie S3**). **(F)** Enlargement of image from box in **E**.

thickness of CSDB sequences is susceptible not only to core orientation with respect to corallum growth orientation (*apparent thickness*) (Worum et al., 2007) but also the multiple effects of seafloor diagenesis. In addition, because clear evidence of diagenetic replacement of the original coral skeletal walls was rarely observed in the present study (**Supplementary Figures S5D–F**), the coral skeleton is considered to be nearly original in composition.

The growth of aragonite cements similar to those within *Porites* coralla form in deep water seafloor environments at rates of 80–100 μm/year (Schroeder and Purser, 1986; Grammer et al., 1993). By analogy, the 80–140 μm-long aragonite cements occluding coral pores in the present study (**Figures 4–15**) may have grown in 1 year or less. Therefore, precipitation of seafloor diagenetic aragonite cements can grow extremely rapidly and therefore dramatically impact both young and old CSDB

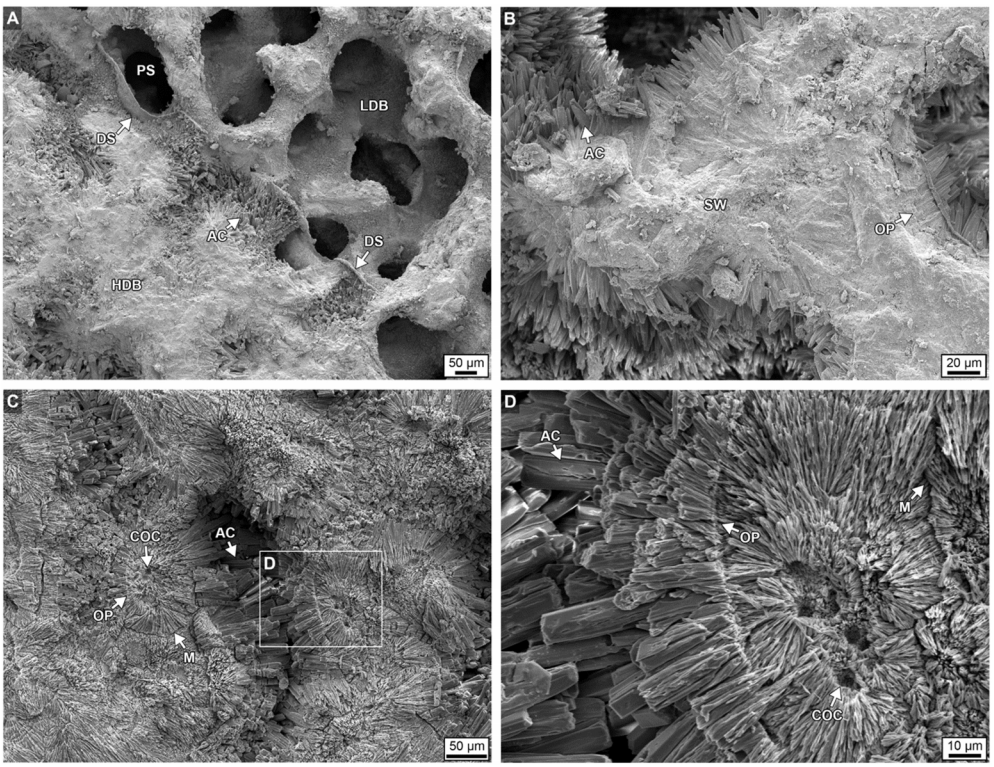

FIGURE 13 | Scanning electron microscope (SEM) images showing extensive diagenetic aragonite cements (AC) occluding pore space within a high-density band (HDB) from the bottom 6 cm of Core 3. **(A,B)** Unetched skeleton. **(C,D)** Skeleton etched in dilute 1% formic acid for 30 s. Labeling includes: PS, pore space; SW, skeletal wall; COC, center of calcification; DS, dissepiments; AC, acicular aragonite cement with both sharp and blunt crystal terminations; OP, original pore margins; and M, contact margins between individual sclerodermites.

sequences. The focus in the present study is placed solely on the effect of diagenetic aragonite cementation on $\delta^{18}O$-derived SST. Similar combined microscopy and modeling approaches can, however, be developed in future studies to include coral skeletal wall replacement if this process is petrographically observed to be influential.

The majority of SST reconstructions from coral skeletons are made from sample powders collected using 1 mm-diameter drill tips [e.g., Sayani et al. (2011)]. To estimate the geochemical impact of mixing diagenetic aragonite cement with original coral skeleton resulting from this microdrilling technique, we combine quantitative petrographic image analyses in the context of the 1 mm-diameter area collected when microdrilling with mass balance modeling (**Figure 15**). To evaluate the reliability of this approach and establish its applicability to tropical reef tracts around the world, petrographic analyses of *Porites* from the Great Barrier Reef in the present study (**Figure 15**) are integrated with $\delta^{18}O$ and Sr/Ca (n = 80) analyses collected from *Porites* in Papua New Guinea [Quinn and Taylor (2006); gray data field in **Figure 15E**]. Images depicting 0, 21, 43, and 53% (the maximum observed) mixtures of diagenetic aragonite cement with original coral skeleton are chosen as specific examples (**Figures 15A–D**). A standard binary mixing curve (**Figure 15E**) is established with endmember geochemical compositions for the original coral aragonite skeleton ($\delta^{18}O$ = −5.5 VPDB; Sr/Ca = 8.7 mmol/mol) and diagenetic aragonite cements ($\delta^{18}O$ = −2.0 VPDB; Sr/Ca = 10.5 mmol/mol; **Figure 15E**). Detailed explanation of the derivation of mixing model equations is presented in Langmuir et al. (1978). Results illustrate the consistent linear covariations of Sr/Ca versus $\delta^{18}O$ as more and more diagenetic aragonite cement is mixed with original coral skeleton (**Figure 15E**). It is important to note that this quantitative establishment of the mixing curve is independent of the processes that control the endmember coral skeleton and diagenetic cement geochemistry. Once the mixing curve is established, we specifically calculated a quantitative correction factor exclusively for the $\delta^{18}O$-derived SST calibration (**Figure 15E**). A Sr/Ca-derived SST correction factor is not presented because Alpert et al. (2016) quantitatively proved that the Sr/Ca content of coral skeletal aragonite can vary independently of the coral skeletal $\delta^{18}O$.

Figure 15E indicates the amount of change in Sr/Ca mmol/mol (x-axis) and $\delta^{18}O$ VPDB (y-axis) created by each extent of mixing. These shifts in isotopic and elemental composition can be used to quantitatively correct coral skeleton-derived SST reconstructions. Application of $\delta^{18}O$ SST paleothermometry calculations (Epstein et al., 1953; Mcculloch et al., 1994; Kim and ONeil, 1997; Gagan et al., 1998; Ren et al., 2002; Cahyarini et al., 2008; Nurhati et al., 2009; Sayani et al., 2011; Kim et al., 2012) indicate SST corrections of

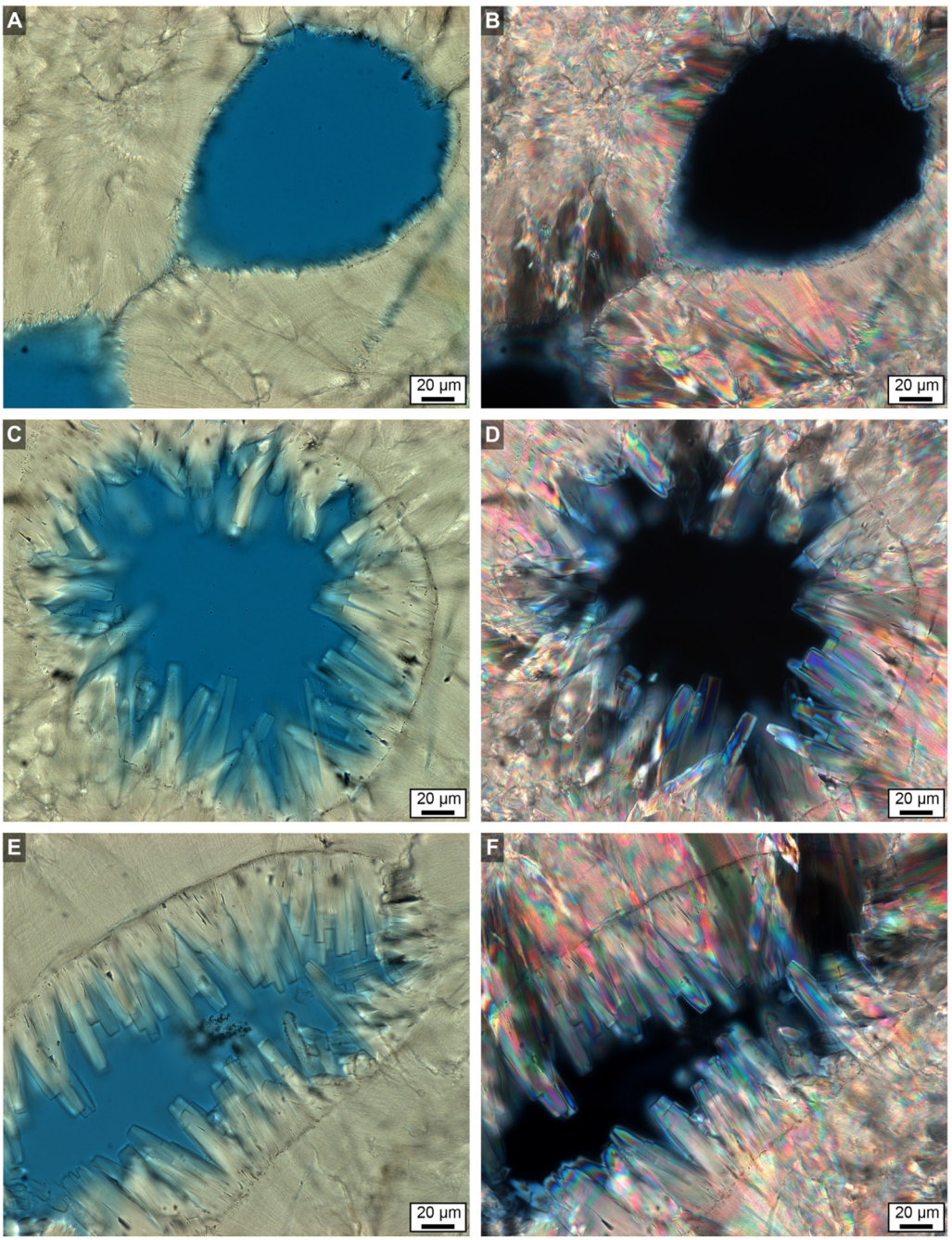

FIGURE 14 | Brightfield (BF) and polarization (POL) images showing extensive diagenetic aragonite cement occluding high- and low-density band (HDB and LDB) pore space in the bottom 6 cm of Core 3. **(A,C,E)** BF images. **(B,D,F)** Corresponding POL images. Original pore margins are clearly visible in all images. Diagenetic aragonite cement exhibits both sharp and blunt crystal terminations. Images **(A,B)** are from a LDB, while images **(C–F)** are from HDBs.

+4.3°C for 21% mixing, +7.4°C for 42% mixing, and +9.3°C for 53% mixing (**Figure 15E**). This is consistent with multiple previous studies, which have inferred but not quantified within the context of CSDB that increasing proportions of diagenetic aragonite cement in the microdrilled powder mixture will serve to artificially depress SST estimates (Mcculloch et al., 1994; Gagan et al., 1998; Enmar et al., 2000; Ren et al., 2002; Quinn and Taylor, 2006; Cahyarini et al., 2008; Nurhati et al., 2009; Sayani et al., 2011). **Figure 15E** further indicates that mixtures of as little as 5% diagenetic aragonite cement result in SST anomalies of 0.9°C, which is an extent of cementation commonly observed in many CSDB intervals. All geochemical diagenetic alteration is toward higher $\delta^{18}O$ VPDB values (**Figure 15E**), implying that seafloor diagenesis

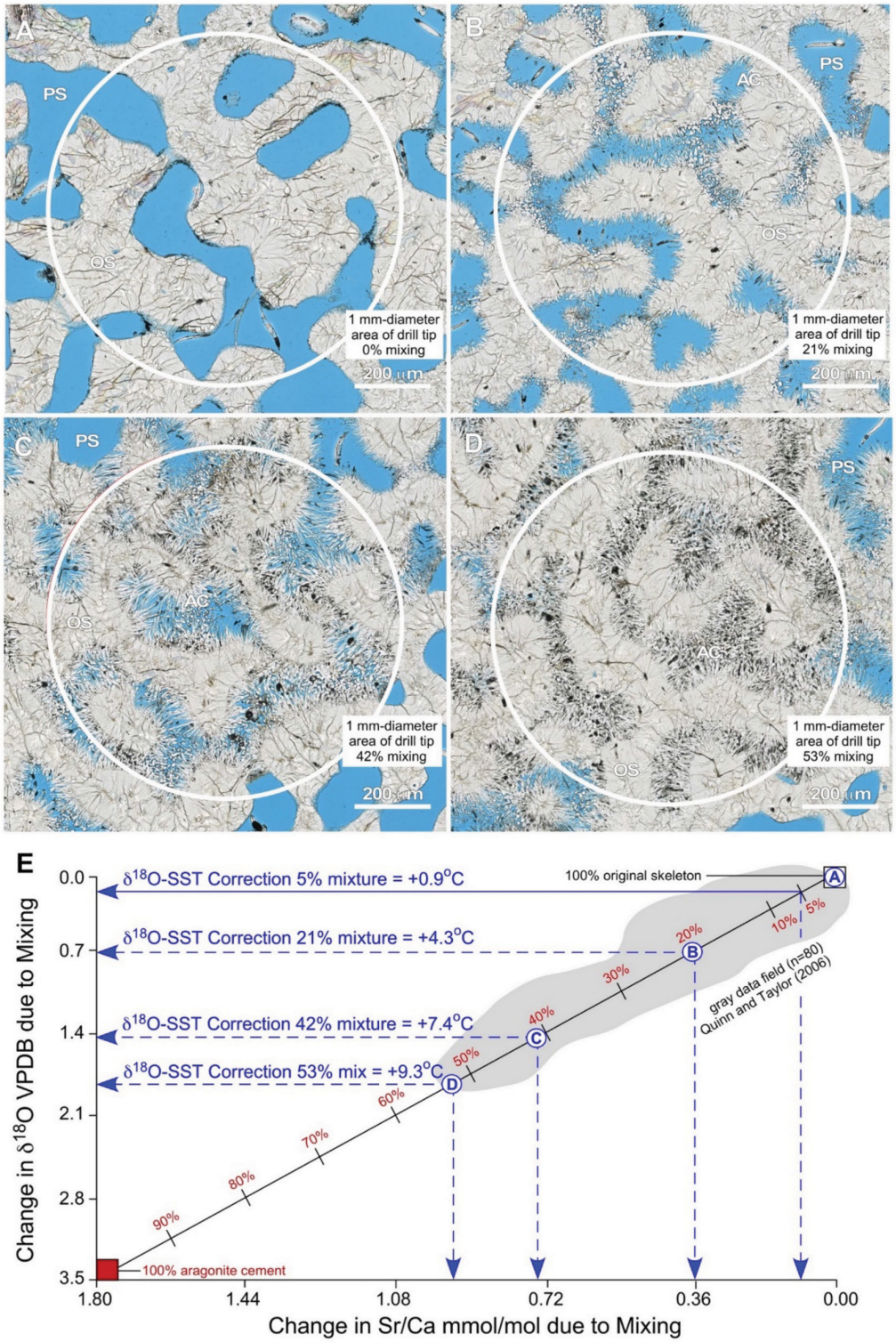

FIGURE 15 | Example integration of quantitative petrography with binary mixing modeling to estimate correction factors for the impact of seafloor diagenesis on δ^{18}O-derived SST reconstructs from coral skeletons. **(A–D)** Nanozoomer BF images of high-density bands (HDBs) located 6 cm above the base of Core 3 (**Figures 2**, **6**). Images of HDBs with 0% **(A)**, 21% **(B)**, 42% **(C)**, and 53% **(D)** cement occlusion are shown. A 1 mm-diameter drill tip (white circles) will yield a microdrilled sample powder composed of a mixture of original coral skeleton (SW) with diagenetic aragonite cements (AC) that grow into and occlude skeletal pore space (PS; black in ring aperture contrast, RAC). **(E)** A binary mixing line [calculated from Langmuir et al. (1978)] shows changing Sr/Ca mmol/mol vs. δ^{18}O VPDB

(Continued)

FIGURE 15 | Continued
with increasing proportions of diagenetic aragonite cements. The extent of mixing is independently and quantitatively determined from microscopy (**A–D**, and **Supplementary Figures S6, S7**). Endmember geochemical compositions for the original *Porites* aragonite skeleton ($\delta^{18}O$ = –5.5 VPDB; Sr/Ca = 8.7 mmol/mol) and diagenetic aragonite cement ($\delta^{18}O$ = –2.0 VPDB; Sr/Ca = 10.5 mmol/mol) are from analyses *Porites* in Papua New Guinea (Quinn and Taylor, 2006). The gray data field (n = 80) is from Quinn and Taylor (2006). The X-axis and Y-axis intercepts indicate the amount of change caused by mixing in Sr/Ca mmol/mol and $\delta^{18}O$ VPDB, respectively. These shifts in isotopic and elemental composition are used to correct SST reconstructions following previously established paleothermometry calculations (Epstein et al., 1953; Kim and ONeil, 1997; Nurhati et al., 2009; Sayani et al., 2011; Kim et al., 2015). Results yield SST corrections of +4.3°C for 21% mixing, +7.4°C for 43% mixing, and +9.3°C for 53% mixing, respectively. Note the strong correlation in data covariation and range with the binary mixing line and the maximum 53% mixing observed in thin-section. Mixtures of as little as 5% diagenetic aragonite cement, which is common in many CSDB intervals, will result in $\delta^{18}O$-derived SST anomalies of 0.9°C.

consistently occurred in seawater that was equivalent to, or cooler than, the temperature of the seawater in which the original coral skeleton was deposited. Similar corrections can be calculated from changes in Sr/Ca (Alibert and McCulloch, 1997). However, Sr/Ca-based SST corrections are not presented here because of the multiple potential influences of local biological vital effects, instrument error, other uncertainties (Alpert et al., 2016) and diagenetic alteration (Enmar et al., 2000; Sadler et al., 2014).

Multiple lines of evidence indicate that this integration of quantitative high-resolution petrography with binary mixing modeling is required in future studies to establish correction factors for $\delta^{18}O$-derived SST (**Figure 15**). The Quinn and Taylor Sr/Ca and $\delta^{18}O$ data set correlates strongly with binary mixing between original skeleton and diagenetic cements in the present study, extending from 0% to approximately 53% mixing (**Figure 15E**). While Quinn and Taylor recognized these relationships, they did not calculate the extent of mixing or associated SST correction factors because detailed high-resolution petrographic analyses of the *Porites* HDBs and LDBs were not available. In addition, the maximum extent of 53% mixing as documented with our image analyses (**Figure 15D**) coincides precisely with the lowest paired analyses of Sr/Ca versus $\delta^{18}O$ from Quinn and Taylor (Quinn and Taylor, 2006; **Figure 15E**). Furthermore, the largest previously documented anomaly of approximately 9°C observed between coral-derived SST and instrument-measured SST (McGregor and Gagan, 2003; Moses et al., 2006; Quinn and Taylor, 2006; Hendy et al., 2007; McGregor and Abram, 2008; Sayani et al., 2011) is consistent with the SST correction of 9.3°C suggested by the maximum extent of 53% mixing observed in thin-section in the present study (**Figures 15D,E**).

Multiple lines of evidence indicate that the integration of high-resolution microscopy with binary mixing models (**Figure 15**) produces reliable quantitative corrections for the impact of seafloor diagenesis on $\delta^{18}O$-derived SST reconstructions made from discrete CSDB stratigraphic intervals. These correction factors can be directly applied to other modern and fossil types of coral, marine invertebrate and plant skeletons, and other marine carbonate proxies (i.e., marine cements, ooids, stromatolites, etc.) (Brand and Veizer, 1981; Veizer, 1983; Fouke et al., 1996). Our findings on Myrmidon Reef demonstrate that seafloor diagenesis has a systematically recurring impact on both CSDB chronostratigraphy and $\delta^{18}O$-derived SST reconstructions within specific CSDB intervals at the base of cores 3 and 4 in deeper seawater.

CONCLUSION

In conclusion, marine carbonate research has shown that variable extents of seafloor diagenetic aragonite cementation (ranging from being absent and rare to common and abundant) possibly takes place within coral skeletons around the world (Berner, 1966; Bathurst, 1974; Schroeder and Purser, 1986; Banner and Hanson, 1990; Morse and Mackenzie, 1990; Tucker et al., 1990; Grammer et al., 1993; Enmar et al., 2000; Hendy et al., 2007; Nothdurft and Webb, 2007). To address the impact of these potential diagenetic influences in future coral-based SST reconstructions, we have established the following systematic approach. This includes: (1) conduct XRD and Micro CT analyses to establish CSDB chronostratigraphy; (2) prepare petrographic thin sections covering as much of the coral skeleton as feasible: and (3) determine the extent to which diagenetic aragonite cementation has taken place using optical and electron microscopy. If this screening indicates that diagenetic aragonite cementation is absent or rare, then no SST correction factors are required. However, if screening indicates that diagenetic aragonite cementation is common to abundant, then correction factors will be beneficial to improve the accuracy of the $\delta^{18}O$-derived SST. This is accomplished by combining the percent of diagenetic aragonite cement as determined from high-resolution petrographic image analysis, with a quantitative mixing model presented here.

CONTRIBUTION TO THE FIELD STATEMENT

This paper, which directly builds upon previous research, is the first to fully contextualize and integrate high-resolution microscopy with mass balance binary mixing models to establish reliable and reproducible correction factors for the impact of seafloor diagenesis on $\delta^{18}O$-derived SST reconstructions. Four cores are analyzed from *Porites* coralla growing at 4–24 m water depth (WD) at Myrmidon Reef, Great Barrier Reef, Australia. This includes detailed study of 35 polished 25 μm-thick thin sections covering a total core length of 2.1 m. While more than 95% of the coral skeletal cores exhibit little to no diagenetic alteration, the bottom several centimeters of the two deeper cores (16 and 24 m WD) contain CSDB intervals of extensive diagenetic

aragonite cementation within original skeletal pore spaces. We derive correction factors for $\delta^{18}O$-derived SST by applying the percent mixing of diagenetic aragonite cement with original skeleton (as determined from high-resolution microscopy) to binary mixing models. These correction factors can be applied to globally distributed CSDB-derived $\delta^{18}O$ and Sr/Ca data sets.

DATA AVAILABILITY

The raw data supporting the conclusions of this manuscript will be made available by the authors, without undue reservation, to any qualified researcher.

AUTHOR CONTRIBUTIONS

MK, KyF, and BF collected the coral cores from Myrmidon Reef. MS, KyF, LT, and BF performed the experiments, analyzed the data, and prepared final images. MS collected and interpreted MicroCT data. MS, KyF, and BF drafted the manuscript. BF supervised the project. MS, KyF, LT, MK, KaF, JT, and BF conducted collaborative research support throughout the study, reviewed and edited the entire manuscript continuously leading up to the submission version.

FUNDING

This research was supported by grants from the National Aeronautics and Space Administration (NASA) Astrobiology Institute (Cooperative Agreement No. NNA13AA91A) issued through the Science Mission Directorate, the Office of Naval Research (N00014-00-1-0609) and the Australian Research Council (ARC) Centre of Excellence for Coral Reef Studies. Coral cores were collected under the Australian Government Great Barrier Reef Marine Park Authority Permit G15/37167.1 issued to MK. Conclusions are those of the authors and may not reflect those of the funding agencies.

ACKNOWLEDGMENTS

We sincerely thank M. O'Callaghan, K. Hartog-Burnett and other members of the Kingsford laboratory at James Cook University for their tireless teamwork in collecting the coral cores on Myrmidon Reef. We also thank G. A. Fried for expertise in preparing and cutting coral cores, E. Fried for assistance with preparation and analysis of the coral cores at the University of Texas Computed Tomography (UTCT) laboratory, and M. W. Colbert and J. Maisano for their extraordinary efforts and expertise in completing the MicroCT analyses at UTCT. K. Lee conducted EDXS analyses at the University of Illinois Urbana–Champaign Beckman Institute. We also thank J. Conroy for advice and suggestions regarding paleothermometry and climate predictions. We are also appreciative to L. Z. DeVille for in-depth discussion on mixing curves and his expertise in mathematic modeling and L. Trevor, Application Engineer, Materials and Structural Analysis Division (MSD) at ThermoFisher Scientific for help with creating the 3-D rendering of corals from MicroCT data using Amira software. We are also thankful to Aaron King at the Department of Geography and Geographic Information Science, University of Illinois at Urbana–Champaign for helping us create high resolution Australia sample location maps using ArcGIS software.

SUPPLEMENTARY MATERIAL

The Supplementary Material for this article can be found online at: https://www.frontiersin.org/articles/10.3389/fmars.2019.00306/full#supplementary-material

REFERENCES

Alibert, C., and McCulloch, M. T. (1997). Strontium/calcium ratios in modern Porites corals from the Great Barrier Reef as a proxy for sea surface temperature: calibration of the thermometer and monitoring of ENSO. *Paleoceanography* 12, 345–363. doi: 10.1029/97pa00318

Allemand, D., Tambutte, E., Zoccola, D., and Tambutte, S. (2011). "Coral calcification, cells to reefs," in *Coral Reefs: An Ecosystem in Transition*. eds Z. Dubinsky and N. Stambler (Dordrecht: Springer), 119–150. doi: 10.1007/978-94-007-0114-4_9

Alpert, A. E., Cohen, A. L., Oppo, D. W., DeCarlo, T. M., Gove, J. M., Young, C. W., et al. (2016). Comparison of equatorial Pacific sea surface temperature variability and trends with Sr/Ca records from multiple corals. *Paleoceanography* 31, 252–265. doi: 10.1002/2015pa002897

Banner, J. L., and Hanson, G. N. (1990). Calculation of simultaneous isotopic and trace-element variations during water-rock interaction with applications to carbonate diagenesis. *Geochim. Cosmochim. Acta* 54, 3123–3137.

Barkley, H. C., Cohen, A. L., Golbuu, V. R., Starczak, Y., DeCarlo, T. M., Shamberger, K. E. F., et al. (2015). Changes in coral reef communities across a natural gradient in seawater pH. *Sci. Adv.* 1:e1500328. doi: 10.1126/sciadv.1500328

Barnes, D. J., and Lough, J. M. (1993). On the nature and causes of density banding in massive coral skeletons. *J. Exp. Mar. Biol. Ecol.* 167, 91–108. doi: 10.1016/0022-0981(93)90186-r

Bathurst, R. G. (1974). Marine diagenesis of shallow-water calcium-carbonate sediments. *Annu. Rev. Earth Planet. Sci.* 2, 257–274. doi: 10.1146/annurev.ea.02.050174.001353

Berner, R. A. (1966). Diagenesis of carbonate sediments: interaction of magnesium in sea water with mineral grains. *Science* 153, 188–191. doi: 10.1126/science.153.3732.188

Blunden, J., and Arndt, D. S. (2016). A Look at. (2017):Takeaway points from the state of the climate supplement. *Bull. Am. Meteorol. Soc.* 98, 1563–1572. doi: 10.1175/bams-d-17-0148.1

Brachert, T. C., Reuter, M., Krüger, S., Böcker, A., Lohmann, H., Mertz-Kraus, R., et al. (2013). Density banding in corals: barcodes of past and current climate change. *Coral Reefs* 32, 1013–1023. doi: 10.1007/s00338-013-1056-7

Brand, U., and Veizer, J. (1980). Chemical diagenesis of a multicomponent carbonate system.1. Trace-elements. *J. Sediment. Petrol.* 50, 1219–1236.

Brand, U., and Veizer, J. (1981). Chemical diagenesis of a multicomponent carbonate system.2. Stable isotopes. *J. Sediment. Petrol.* 51, 987–997.

Budd, A. F., Fukami, H., Smith, N. D., and Knowlton, N. (2012). Taxonomic classification of the reef coral family Mussidae (Cnidaria: Anthozoa:

Scleractinia). *Zool. J. Linn. Soc. Lond.* 166, 465–529. doi: 10.1111/j.1096-3642.2012.00855.x

Cahyarini, S. Y., Pfeiffer, M., Timm, O., Dullo, W. C., and Schonberg, D. G. (2008). Reconstructing seawater delta(18)O from paired coral delta(18)O and Sr/Ca ratios: methods, error analysis and problems, with examples from Tahiti (French Polynesia) and Timor (Indonesia). *Geochim. Cosmochim. Acta* 72, 2841–2853. doi: 10.1016/j.gca.2008.04.005

Cohen, A. L., and Hart, S. R. (2004). Deglacial sea surface temperatures of the western tropical Pacific: a new look at old coral. *Paleoceanography* 19:A4031.

Cohen, A. L., and McConnaughey, T. A. (2003). Geochemical perspectives on coral mineralization. *Rev. Mineral. Geochem.* 54, 151–187. doi: 10.2113/0540151

Correge, T. (2006). Sea surface temperature and salinity reconstruction from coral geochemical tracers. *Palaeogeogr. Palaeocl.* 232, 408–428. doi: 10.1016/j.palaeo.2005.10.014

Cromey, D. W. (2010). Avoiding twisted pixels: ethical guidelines for the appropriate use and manipulation of scientific digital images. *Sci. Eng. Ethics* 16, 639–667. doi: 10.1007/s11948-010-9201-y

Crowley, T. J., Quinn, T. M., and Hyde, W. T. (1999). Validation of coral temperature calibrations. *Paleoceanography* 14, 605–615. doi: 10.1029/1999pa900032

Cuif, J. P., and Dauphin, Y. (2005). The Environment Recording Unit in coral skeletons - a synthesis of structural and chemical evidences for a biochemically driven, stepping-growth process in fibres. *Biogeosciences* 2, 61–73. doi: 10.5194/bg-2-61-2005

Darke, W. M., and Barnes, D. J. (1993). Growth trajectories of corallites and ages of polyps in massive colonies of reef-building corals of the genus porites. *Mar. Biol.* 117, 321–326. doi: 10.1007/bf00345677

De'ath, G., Lough, J. M., and Fabricius, K. E. (2009). Declining coral calcification on the Great Barrier Reef. *Science* 323, 116–119. doi: 10.1126/science.1165283

DeCarlo, T. M., and Cohen, A. L. (2017). Dissepiments, density bands and signatures of thermal stress in Porites skeletons. *Coral Reefs* 36, 749–761. doi: 10.1007/s00338-017-1566-9

DeCarlo, T. M., Comeau, S., Cornwall, C. E., and McCulloch, M. T. (2018). Coral resistance to ocean acidification linked to increased calcium at the site of calcification. *Proc. Roy. Soc. B Biol. Sci.* 285, 20180564. doi: 10.1098/rspb.2018.0564

DeLong, K. L., Quinn, T. M., and Taylor, F. W. (2007). Reconstructing twentieth-century sea surface temperature variability in the southwest Pacific: a replication study using multiple coral Sr/Ca records from New Caledonia. *Paleoceanography* 22:A4212.

Enmar, R., Stein, M., Bar-Matthews, M., Sass, E., Katz, A., Lazar, B., et al. (2000). Diagenesis in live corals from the Gulf of Aqaba. I. The effect on paleo-oceanography tracers. *Geochim. Cosmochim. Acta* 64, 3123–3132. doi: 10.1016/s0016-7037(00)00417-8

Epstein, S., Buchsbaum, R., Lowenstam, H. A., and Urey, H. C. (1953). Revised carbonate-water isotopic temperature scale. *Geol. Soc. Am. Bull.* 64, 1315–1325.

Eyre, B. D., Cyronak, T., Drupp, P., De Carlo, E. H., Sachs, J. P., Andersso, N. A. J., et al. (2018). Coral reefs will transition to net dissolving before end of century. *Science* 359, 908–911. doi: 10.1126/science.aao1118

Fantazzini, P., Mengoli, S., Pasquini, L., Bortolotti, V., Brizi, L., Mariani, M., et al. (2015). Gains and losses of coral skeletal porosity changes with ocean acidification acclimation. *Nat. Commun.* 6:7785. doi: 10.1038/ncomms8785

Fouke, B. W., Beets, C. J., Meyers, W. J., Hanson, G. N., and Melillo, A. J. (1996). Sr-87/Sr-86 chronostratigraphy and dolomitization history of the seroe domi formation, curacao (Netherlands Antilles). *Facies* 35, 293–320. doi: 10.1007/bf02536966

Frankowiak, K., Mazur, M., Gothmann, A. M., and Stolarski, J. (2013). Diagenetic alteration of triassic coral from the aragonite konservat-lagerstatte in alakir cay, turkey: implications for geochemical measurements. *Palaios* 28, 333–342. doi: 10.2110/palo.2012.p12-116r

Gagan, M. K., Ayliffe, L. K., Hopley, D., Cali, J. A., Mortimer, G. E., Chappell, J., et al. (1998). Temperature and surface-ocean water balance of the mid-Holocene tropical Western Pacific. *Science* 279, 1014–1018. doi: 10.1126/science.279.5353.1014

Gower, L. B. (2008). Biomimetic model systems for investigating the amorphous precursor pathway and its role in biomineralization. *Chem. Rev.* 108, 4551–4627. doi: 10.1021/cr800443h

Grammer, G. M., Ginsburg, R. N., Swart, P. K., McNeil, D. F., Jull, A. J. T., Prezbindowski, D. R., et al. (1993). Rapid growth-rates of syndepositional marine aragonite cements in steep marginal slope deposits, bahamas and Belize. *J. Sediment. Petrol.* 63, 983–989.

Hendy, E. J., Gagan, M. K., Lough, J. M., McCulloch, M., and deMenocal, P. B. (2007). Impact of skeletal dissolution and secondary aragonite on trace element and isotopic climate proxies in Porites corals. *Paleoceanography* 22:A4101.

Hoegh-Guldberg, O., Mumby, P. J., Hooten, A. J., Steneck, R. S., Greenfield, P., Gomez, E., et al. (2007). Coral reefs under rapid climate change and ocean acidification. *Science* 318, 1737–1742.

Holcomb, M., Cohen, A. L., Gabitov, R. I., and Hutter, J. L. (2009). Compositional and morphological features of aragonite precipitated experimentally from seawater and biogenically by corals. *Geochim. Cosmochim. Acta* 73, 4166–4179. doi: 10.1016/j.gca.2009.04.015

Hughes, T. P. (1987). Skeletal Density and Growth Form of Corals. *Mar. Ecol. Prog. Ser.* 35, 259–266. doi: 10.3354/meps035259

IPCC. (2018). *Global Warming of 1.5 degree C*. Geneva: IPCC.

Kandianis, M. T., Fouke, B. W., Johnson, R. W., Veysey, J., and Inskeep, W. P. (2008). Microbial biomass: a catalyst for CaCO3 precipitation in advection-dominated transport regimes. *Geol. Soc. Am. Bull.* 120, 442–450. doi: 10.1130/b26188.1

Kim, S. T., Coplen, T. B., and Horita, J. (2015). Normalization of stable isotope data for carbonate minerals: implementation of IUPAC guidelines. *Geochim. Cosmochim. Acta* 158, 276–289. doi: 10.1016/j.gca.2015.02.011

Kim, S. T., and ONeil, J. R. (1997). Equilibrium and nonequilibrium oxygen isotope effects in synthetic carbonates. *Geochim. Cosmochim. Acta* 61, 3461–3475. doi: 10.1016/s0016-7037(97)00169-5

Kim, W., Fouke, B. W., Petter, A. L., Quinn, T. M., Kerans, C., Taylor, F., et al. (2012). Sea-level rise, depth-dependent carbonate sedimentation and the paradox of drowned platforms. *Sedimentology* 59, 1677–1694. doi: 10.1111/j.1365-3091.2012.01321.x

Kitano, Y. F., Benzoni, F., Arrigoni, R., Shirayama, Y., Wallace, C. C., Fukami, H., et al. (2014). A phylogeny of the family poritidae (Cnidaria, Scleractinia) based on molecular and morphological analyses. *PloS One* 9:e98406. doi: 10.1371/journal.pone.0098406

Knutson, D. W., Buddemeier, R. W., and Smith, S. V. (1972). Coral chronometers: seasonal growth bands in reef corals. *Science* 177, 270–272. doi: 10.1126/science.177.4045.270

Langmuir, C. H., Vocke, R. D., Hanson, G. N., and Hart, S. R. (1978). General mixing equation with applications to icelandic basalts. *Earth Planet. Sci. Lett.* 37, 380–392. doi: 10.1016/0012-821x(78)90053-5

Laudan, R. (1987). *From mineralogy to geology : the foundations of a science,. (1650)-1830. Science and its conceptual foundations*. Chicago: University of Chicago Press, 278.

Lough, J. M., and Barnes, D. J. (1989). Possible relationships between environmental variables and skeletal density in a coral colony from the central Great-Barrier-Reef. *J. Exp. Mar. Biol. Ecol.* 134, 221–241. doi: 10.1016/0022-0981(89)90071-3

Lough, J. M., and Barnes, D. J. (2000). Environmental controls on growth of the massive coral Porites. *J. Exp. Mar. Biol. Ecol.* 245, 225–243. doi: 10.1016/s0022-0981(99)00168-9

Mass, T., Giuffre, A. J., Sun, C. Y., Stifler, C. A., Frazier, M. J., Neder, M., et al. (2017). Amorphous calcium carbonate particles form coral skeletons. *Proc. Natl. Acad. Sci. U.S.A.* 114, E7670–E7678. doi: 10.1073/pnas.1707890114

Mcculloch, M. T., Gagan, M. K., Mortimer, G. E., Chivas, A. R., and Isdale, P. J. (1994). High-Resolution Sr/Ca and Delta-O-18 coral record from the Great-Barrier-Reef, Australia, and the 1982-1983 El-Nino. *Geochim. Cosmochim. Acta* 58, 2747–2754. doi: 10.1016/0016-7037(94)90142-2

McGregor, H. V., and Abram, N. J. (2008). Images of diagenetic textures in Porites corals from Papua New Guinea and Indonesia. *Geochem. Geophy. Geosyst.* 9:Q10013.

McGregor, H. V., and Gagan, M. K. (2003). Diagenesis and geochemistry of porites corals from Papua New Guinea: implications for paleoclimate reconstruction. *Geochim. Cosmochim. Acta* 67, 2147–2156. doi: 10.1016/s0016-7037(02)01050-5

McIlreath, I. A., and Morrow, D. W. (1990). *Diagenesis*. St. John's: Geological Association of Canada, 338.

Morse, J. W., and Mackenzie, F. T. (1990). *Geochemistry of Sedimentary Carbonates. Developments in sedimentology*, Vol. 48. Amsterdam: Elsevier, 707.

Moses, C. S., Swart, P. K., and Dodge, R. E. (2006). Calibration of stable oxygen isotopes in Siderastrea radians (Cnidaria : Scleractinia): implications for slow-growing corals. *Geochem. Geophy Geosyst.* 7:Q09007.

Muller, A., Gagan, M. K., and Lough, J. M. (2004). Effect of early marine diagenesis on coral reconstructions of surface-ocean C-13/C-12 and carbonate saturation state. *Global Biogeochem. Cycles* 18:GB1033.

NASA-GISS (2018). Available at: https://www.giss.nasa.gov/research/features/201708_hotjuly/ (accessed July 4, 2018).

NOAA-NCDC (2018). Available at: https://www.ncdc.noaa.gov/climate-information/extreme-events (accessed July 4, 2018).

Nothdurft, L. D., and Webb, G. E. (2007). Microstructure of common reef-building coral genera Acropora, Pocillopora, Goniastrea and Porites: constraints on spatial resolution in geochemical sampling. *Facies* 53, 1–26. doi: 10.1007/s10347-006-0090-0

Nurhati, I. S., Cobb, K. M., Charles, C. D., and Dunbar, R. B. (2009). Late 20th century warming and freshening in the central tropical Pacific. *Geophys. Res. Lett.* 36:L21606.

Ogilvie, M. M. (1896). Microscopic and systematics study of madreporarian types of corals. *Philos.Trans.R.Soc. Lond.*29, 83–345. doi: 10.1098/rstb.1896.0003

Perrin, C., and Smith, D. C. (2007). Earliest steps of diagenesis in living scleractinian corals: evidence from ultrastructural pattern and Raman spectroscopy. *J. Sediment. Res.* 77, 495–507. doi: 10.2110/jsr.2007.051

Piggot, A. M., Fouke, B. W., Sivaguru, M., Sanford, R. A., and Gaskins, H. R. (2009). Change in zooxanthellae and mucocyte tissue density as an adaptive response to environmental stress by the coral, Montastraea annularis. *Mar. Biol.* 156, 2379–2389. doi: 10.1007/s00227-009-1267-1

Potthast, I. (1992). Short-term progressive early diagenesis in density bands of recent corals: porites colonies, Mauritius Island, Indian Ocean. *Facies* 27, 105–112.

Pratz, E. (1882). ueber die verwandtschaftlichen bezihungen einiger korallengattungen mit hauptsaechlicher berueckichtigung iher septalstructur. *Palaeontographica* 29, 81–122.

Quinn, T. M., and Taylor, F. W. (2006). SST artifacts in coral proxy records produced by early marine diagenesis in a modern coral from Rabaul, Papua New Guinea. *Geophys. Res. Lett.* 33:L04601.

Ren, L., Linsley, B. K., Wellington, G. M., Schrag, D. P., and Hugh-Guldberg, O. (2002). Deconvolving the 18O seawater component from subseasonal coral 18O and Sr/Ca at Rarotonga in the southwestern subtropical Pacific for the period 1726 to 1997. *Geochim. Cosmochim. Acta* 67, 1607–1621.

Sadler, J., Webb, G. E., Nothdurft, L. D., and Dechnik, B. (2014). Geochemistry-based coral palaeoclimate studies and the potential of 'non-traditional' (non-massive Porites) corals: recent developments and future progression. *Earth Sci. Rev.* 139, 291–316. doi: 10.1016/j.earscirev.2014.10.002

Sayani, H., Cobb, K., Cohen, A., Elliott, W. C., Nurhati, I., Rose, K., et al. (2011). Effects of diagenesis on paleoclimate reconstructions from modern and young fossil corals. *Geochim. Cosmochim. Acta* 75, 6361–6373. doi: 10.1016/j.gca.2011.08.026

Schroeder, J. H., and Purser, B. H. (1986). *Reef Diagenesis*. Berlin: Springer-Verlag Heidelberg.

Sivaguru, M., Mander, L., Fried, G., and Punyasena, S. W. (2012). Capturing the surface texture and shape of pollen: a comparison of microscopy techniques. *PLoS One* 7:e39129. doi: 10.1371/journal.pone.0039129

Sivaguru, M., Saw, J. J., Williams, J. C. Jr., Lieske, J. C., Krambeck, A. E., Romero, M. F., et al. (2018a). Geobiology reveals how human kidney stones dissolve in vivo. *Sci.Rep.*8:13731. doi: 10.1038/s41598-018-31890-9

Sivaguru, M., Urban, M. A., Fried, G., Wesseln, C. J., Mander, L., Punyasena, S. W., et al. (2018b). Comparative performance of airyscan and structured illumination superresolution microscopy in the study of the surface texture and 3D shape of pollen. *Microsc. Res. Techn.* 81, 101–114. doi: 10.1002/jemt.22732

Smith, E. G., D'Angelo, C., Sharon, Y., Tchernov, D., and Wiedenmann, J. (2017). Acclimatization of symbiotic corals to mesophotic light environments through wavelength transformation by fluorescent protein pigments. *Proc. Biol. Sci.* 284:20170320. doi: 10.1098/rspb.2017.0320

Stolarski, J., and Roniewicz, E. (2001). Towards a new synthesis of evolutionary relationships and classification of scleractinia. *J. Paleontol.* 75, 1090–1108. doi: 10.1666/0022-3360(2001)075<1090:tansoe>2.0.co;2

Tucker, M. E., Wright, V. P., and Dickson, J. A. D. (1990). *Carbonate Sedimentology*. Oxford: Blackwell Scientific Publications, 482.

Veizer, J. (1983). "Chemical Diagenesis of Carbonates: theory and Application of Trace Elment Techniques," in *Stable Isotopes in Sedimentary geology*, eds M. A. Arthur and T. J. Anderson (Tulsa: Society of Economic Paleontologists and Mineralogists), 3–100.

Venn, A. A., Tambutté, E., Holcomb, M., Laurent, J., Allemand, D., Tambutté, S., et al. (2013). Impact of seawater acidification on pH at the tissue-skeleton interface and calcification in reef corals. *Proc. Natl. Acad. Sci. U.S.A.* 110, 1634–1639. doi: 10.1073/pnas.1216153110

Von Euw, S., Zhang, Q., Manichev, V., Murali, N., Gross, J., Feldman, L. C., et al. (2017). Biological control of aragonite formation in stony corals. *Science* 356, 933–938. doi: 10.1126/science.aam6371

Walther, B. D., Kingsford, M. J., and McCulloch, M. T. (2013). Environmental records from great barrier reef corals: inshore versus offshore drivers. *PLoS One* 8:e77091. doi: 10.1371/journal.pone.0077091

Weiner, S., and Addadi, L. (2011). Crystallization pathways in biomineralization. *Annu. Rev. Mater Res.* 41, 21–40. doi: 10.1146/annurev-matsci-062910-095803

Wells, J. W. (1963). Coral growth and geochronometry. *Nature* 197:948. doi: 10.1038/197948a0

Worum, F. P., Carricart-Ganivet, J. P., Benson, L., and Golicher, D. (2007). Simulation and observations of annual density banding in skeletons of Montastraea (Cnidaria : Scleractinia) growing under thermal stress associated with ocean warming. *Limnol. Oceanogr.* 52, 2317–2323. doi: 10.4319/lo.2007.52.5.2317

Conflict of Interest Statement: The authors declare that the research was conducted in the absence of any commercial or financial relationships that could be construed as a potential conflict of interest.